Climatic Equilibrium of the Atmospheric Convective Boundary Layer over a Tropical Ocean

ALAN K. BETTS
Middlebury, Vermont

W. RIDGWAY
Applied Research Corporation, Landover, Maryland

(Manuscript received 9 December 1988, in final form 10 March 1989)

ABSTRACT

A one-dimensional thermodynamic model for a partially mixed, partly cloudy, convective boundary layer (CBL) is coupled to a radiation model to compute equilibrium solutions for a tropical CBL and troposphere in energy balance over the ocean. For a sea surface temperature (SST) of 300 K, the model gives an equilibrium cloud base $\approx$ 950 mb, a CBL top $\approx$ 800 mb and a low level $\theta_e \approx$ 347 K, close to climatic values. The CBL deepens and low level θ_e rises with increasing wind speed and SST. We explore the change in CBL structure and surface fluxes with external parameters on three timescales; namely, the CBL ($\sim$1 day); the tropospheric radiative equilibrium ($\sim$10 days); and the oceanic thermal equilibrium (>100 days). The variation in cloud top decreases with greater coupling to atmosphere and ocean. The slope of the latent heat flux with increasing SST decreases with more tropospheric coupling, and reverses sign with a coupled ocean. This simplified model gives an increase of tropical SST with a doubling of CO_2 on climatic timescales of 2–3° K, increasing with upper tropospheric moisture.

1. Introduction

A convective boundary layer (CBL) of shallow nonprecipitating cumulus clouds covers most of the tropical oceans away from the atmospheric convergence zones. It is remarkably uniform with the cloud base near 950 mb, an inversion above the top of the cloud layer near 800 mb (e.g., Firestone and Albrecht 1986); and a subcloud layer equivalent potential temperature (θ_e), typically in the range 345–350 K. This boundary layer in turn feeds the deep convection in the ascending branches of the Hadley and Walker circulations, so that the height of the tropopause and tropical tropospheric temperature is directly coupled to the θ_e of the CBL over the oceans (Sarachik 1978). This rather stable equilibrium is a result of a subtle balance between the radiation field, the subsidence, the convective fluxes, the cloud field, the surface wind and the sea surface temperature. This paper addresses this equilibrium balance on three timescales over the oceans, using a simple energy balance model. We shall explore the dependence of the equilibrium low level θ_e, height of cloud base and CBL top, and the surface fluxes of heat and moisture, on sea surface temperature, surface wind speed, and the moisture above the CBL. We then investigate the response of the model on long timescales to simple climate change experiments.

The early studies of the trade winds emphasized the downstream moistening and rise of the top of the cloud layer on equatorward trajectories towards Hawaii (Riehl et al. 1951; Malkus 1956). We shall show that this is largely an equilibrium response to the rise of sea surface temperature along the trajectory. Over most of the tropical Pacific, where the sea surface temperature has weaker gradients, the CBL top is near 800 mb. These early papers used kinematic methods to estimate the mean subsidence in the trades and found values $\approx$ 6 mb day^{-1}, much lower than that required for mass balance in the subsiding branch of the Hadley circulation. Neiburger (1960), however, used trajectories and a radiative budget to estimate the subsidence at CBL top to be $\approx$40 mb day^{-1}. Subsequent mass budget studies of the trade winds in the Atlantic (Holland and Rasmusson 1973; Nitta and Esbensen 1974; Augstein et al. 1973) confirmed that the subsidence in the trade inversion was of order 40–60 mb day^{-1}. Sarachik (1978) and Betts and Ridgway (1988, hereafter referred to as BR) showed that the radiatively driven subsidence in the subsiding branches of the mean tropical circulation was of this same magnitude $\approx$ 40 mb day^{-1}. Betts and Ridgway used a coupled radiative–CBL model and observed CBL data over the equatorial Pacific (Betts and Albrecht 1987) to show that on climatic

Corresponding author address: Alan K. Betts, RD2 Box 3300, Middlebury, Vermont 05753.

timescales, the radiation field was the primary control on the surface fluxes. Because the CBL is the link between the surface sensible and latent heat fluxes and the drier subsiding air above, the proper representation of its depth and thermodynamic structure is important in global forecast and climate models (Heckley 1985; Albrecht et al. 1986). Above cloud base, the CBL is typically not well mixed, but its bulk thermodynamic structure can be represented by a mixing line parameterization (Betts 1986), which will be used here.

There have been many modeling studies of the trade winds, and the shallow cumulus layer in general (Riehl et al. 1951; Malkus 1956; Betts 1973, 1975; Augstein et al. 1973; Ogura et al. 1977; Augstein and Wendel 1980; Hanson 1981, 1987; Albrecht 1984); but only a few have attempted to understand the coupling of the convective and radiative transports (Sarachik 1978, Albrecht et al. 1979; Albrecht 1979). From a climatic viewpoint the oceanic convective boundary layer can be regarded as a specific example of the radiative-convective equilibrium problem, which has been studied largely for the global troposphere (e.g., Ramanathan 1981).

In this paper, we carry the analysis of BR further; that is, by coupling a thermodynamic model for a partially mixed CBL (with a specified cloud fraction) with a radiation model we compute equilibrium solutions for a tropical CBL, troposphere and ocean in energy balance with increasing degrees of coupling. The balance between the radiation field and the CBL structure is quite complex, because radiative cooling has several roles. Above the CBL the subsidence is close to radiative balance. This subsidence continually brings down dry and warm air into the CBL. For the CBL as a whole, radiative cooling largely balances the warming by subsidence (and the smaller surface sensible heat flux), while the upward advection and evaporation of liquid water maintains the sharp temperature inversion (Betts 1973, 1975). Over a uniform ocean, it is the radiative cooling that keeps the subcloud layer cooler than the ocean. This maintains the surface layer instability and the surface sensible (and latent) heat fluxes. In the moisture balance, the subsidence of dry air is balanced by the upward flux of moisture at the surface. The resulting equilibrium moisture structure and associated cloud fields play an important role in controlling the longwave radiative cooling and the net incoming shortwave radiation [the inversion is partly maintained by the radiative perturbation associated with the clouds (BR)]. Finally, the balance of the net incoming radiation and the fluxes of sensible and latent heat at the surface (as well as the oceanic heat transports) determine, on long timescales, the sea surface temperature.

This paper explores sequentially the impact of this radiative coupling on the CBL structure and fluxes on three timescales. After introducing the boundary layer model, the radiation model and the energy balance constraints, we first show the sensitivity of the CBL equilibrium structure and fluxes to external parameters, such as sea surface temperature (SST), surface wind, and a specified upper tropospheric structure and subsidence. The timescale of this response is of the order of a day or two (Schubert et al. 1979). We shall call this the "CBL timescale"; and all the solutions with a specified SST and troposphere above the CBL, the "uncoupled" solutions. We then introduce energy balance for the troposphere, and couple the temperature and moisture structure of the troposphere to the low level θ_e, to give "tropospheric coupled" equilibrium solutions for the CBL. These are representative of a "tropospheric radiative timescale" of order 10 days. On this timescale we shall still regard the SST as an independent specified parameter. These are a new class of solutions which show the coupling of CBL structure and fluxes to specified surface wind and SST on this timescale. Finally, we introduce a further energy balance criterion at the ocean surface to determine the equilibrium SST (Sarachik 1978), and give "ocean coupled" solutions representative of an "oceanic timescale" of order months to years (>100 days). We specify CBL cloud fraction and the oceanic energy transport out of the tropics to give a realistic mean SST, and show the sensitivity of the CBL to changing surface wind, tropopause humidity, solar constant and doubling CO_2. This study, which has a fixed stratosphere, specified ocean transports, and no atmospheric transports out of the tropics, has limitations as a climate model; but these sensitivity studies are shown for comparison with one-dimensional climate models, which often have simpler representations of the CBL, and the fully interactive results from general circulation models. The changing response of the equilibrium CBL and the surface fluxes to increasing coupling with the atmosphere and ocean is then discussed.

2. Theoretical model

a. Concept

Our model is an extension of BR, which was itself based on the single cell model for a tropical circulation in equilibrium proposed by Sarachik (1978). Figure 1 shows the schematic circulation of this single-cell tropical model with a characteristic set of parameters for illustration (from our coupled equilibrium solution: discussed later). We suppose that most of the tropics are covered by a uniform CBL, above a uniform ocean. This is the region we model; not the narrow ascending branch of the deep convection. Figure 1 shows a characteristic set of fluxes, and the radiative flux divergences for the subcloud layer (ΔN_B), the CBL (ΔN_T) and the troposphere (ΔN_{TR}), which will play an important role in the budget analysis. We shall neglect X_A (marked with asterisk), the atmospheric export from the tropics, because it is partly balanced by the warming effect of upper level clouds which we also neglect; and in later sections we shall specify X_O, the oceanic export, to give

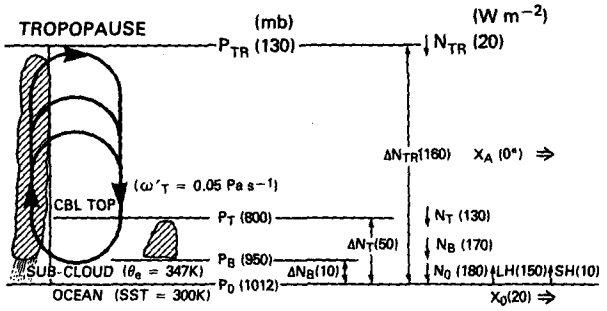

FIG. 1. Schematic showing single cell tropical circulation, and selected values from the equilibrium solution with a coupled atmosphere and ocean (see text).

a realistic SST with a specified cloud fraction consistent with observations [see section 2h(3)].

In this section we shall outline the components of the model in turn. The primary focus of the paper is the CBL equilibrium on different timescales. The CBL model is based on the mixing line representation of clear and cloudy thermodynamic profiles for a shallow cumulus layer suggested in Betts (1985, 1986), and discussed in the next section. The surface fluxes are parameterized by bulk aerodynamic formulae. The troposphere above the CBL has a moist adiabatic *temperature* structure, which in the troposphere and ocean coupled solutions lies on the moist θ_{es} adiabat through a low level θ_e, (2 mb above the surface) and in the uncoupled CBL solution follows a specified moist adiabat. The tropospheric moisture *profile* above the CBL is specified, and in the coupled solutions it is linked to the low level θ_e also. One simplification we shall make is to specify a tropical stratosphere with a constant temperature of 195 K between 100 mb and the tropopause. The tropopause is at the pressure where the θ_{es} adiabat for the troposphere reaches 195 K, and is typically in the range 110–150 mb as θ_e decreases. The radiation model is the extension of Harschvardhan et al. (1987), discussed in BR. It is used to compute net shortwave and longwave fluxes for a clear atmosphere, and one with a specified fraction of plane parallel clouds in the CBL.

The CBL heat and moisture budgets and three energy balance criteria are used to give equilibrium solutions. The CBL thermal budget gives an equilibrium solution for the boundary layer depth in terms of the radiative cooling of the CBL, and the subsidence and temperature at the CBL top. We use a subcloud layer energy balance criteria as a constraint on the surface sensible heat flux, and Bowen ratio. Energy balance for the troposphere determines the subsidence at CBL top, and the CBL equilibrium structure on the atmospheric radiative timescale of order 10 days (section 2h). On oceanic timescales of months to years, we introduce a further constraint on the net flux at the sea surface (and tropopause) to give the equilibrium SST.

b. *Mixing line model for an idealized CBL*

The CBL is typically not well mixed, particularly above cloud base. However, its bulk thermodynamic structure can conveniently be approximated by a mixing line representation (Betts 1982a,b, 1985, 1986). Idealized but quite realistic thermodynamic profiles can be constructed with a mixing line model, using different bulk parameters to represent clouds and the clear regions between them. Figure 2 shows example profiles on a thermodynamic diagram for the tropospherically coupled solution with SST = 300 K. A mixing line (heavy dashes) is computed between air near the ocean surface with properties (θ_{MO}, q_{MO}), and the air just above the CBL with properties (θ_T, q_T); see Betts 1982a. All the air in the CBL is presumed to have thermodynamic properties lying on this mixing line. We then construct the thermodynamic profiles for clear and cloudy air within the CBL by specifying different profiles for a parameter

$$\beta = dp^*/dp \qquad (1)$$

the change of saturation level with pressure along the mixing line (Betts 1982b, 1985). We compute separate clear and cloudy profiles by using two pairs of values for β. For the clear air environment between clouds (solid lines in Fig. 2) we specified β_u = 0.2, 1.2 below cloud base and above cloud base respectively, (up to the inversion base), consistent with observations of the CBL structure over the oceans (Betts and Albrecht 1987). The resolved inversion layer thickness was fixed at 20 mb, with a linear transition of p^* across it. For the cloudy CBL profiles (short dashes), we specified β_c = 0.0, 0.6 below cloud base and in the cloud layer, respectively (up to the inversion base). The value of β_c = 0 gives a well mixed subcloud layer beneath clouds,

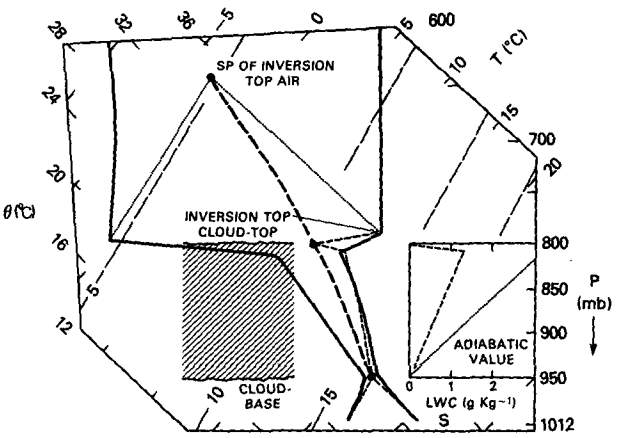

FIG. 2. Tephigram showing CBL model thermodynamic structure. The clear air temperature and mixing ratio are shown as heavy solid lines, and the cloudy air profiles by short dashed lines (the liquid water profile as an insert). The mixing line between the base of the subcloud layer (2 mb above the sea surface) and the air above the inversion is shown as a heavy dashed line.

so that cloud base (generally not a model level) corresponds to the LCL of the air just above the surface. Above cloud base, $\beta_c = 0.6$ gives a cloud layer liquid water profile that is 40% of the adiabatic value, (corresponding to $1 - \beta_c$) to represent the subadiabatic values typical of shallow cumulus clouds. The inset on Fig. 2 shows this liquid water profile. Cloud liquid water is specified to fall to zero (where $p^* = p$), 10 mb above the inversion base, so that we have a well-defined cloud top at the middle of the inversion, where the temperature of the evaporating cloud top can be computed. (It is used in the radiative code.) This temperature lies, as shown, on the mixing line at the cloud top pressure (Betts 1982a).

As Fig. 2 shows, this representation gives us idealized, but realistic, clear and cloudy profiles: with a nearly well mixed subcloud layer, and a conditionally unstable cloud layer capped by an inversion. It can be regarded as an extension of the mixed layer CBL to a partially mixed structure. This is still a bulk parameterization of the CBL because we *specify* the values of β, to be consistent with observations of CBL structure. Our results are not sensitive to this specification. The value of a bulk parameterization is that it gives us realistic thermodynamic profiles (including liquid water) for the radiation computation, which depend only on four *boundary* parameters θ_{MO}, q_{MO} and θ_T, q_T, which can be computed from the budget equations. The mixing line representation gives simple integrated CBL thermodynamic budgets, and it is sufficiently simple to be used to parameterize shallow convection in large-scale numerical models (Betts 1986). Our model vertical resolution was fixed at 10 mb within the CBL for the computation of the radiative fluxes. The solution of the budget equations (see sections 2c to 2h) returns a value of cloud base p_B, and CBL top pressure, p_T, between model levels. The adjacent model levels at cloud top and inversion top were chosen to bracket the computed CBL top pressure, so that the radiating cloud top is within the CBL. Above the CBL top ($p < 790$ mb), the temperature profile in Fig. 2 for this coupled solution follows a moist adiabat through the cloud base temperature, and hence the low level θ_e.

c. Convective boundary layer (CBL) budgets

The steady-state, horizontally homogeneous heat and moisture budgets for the CBL in a subsiding mean flow can be written

$$\omega(T/\theta)\partial\theta/\partial p - (g/C_p)\partial N/\partial p - g(T/\theta)\partial F_\theta/\partial p = 0 \quad (2a)$$

$$\omega\partial q/\partial p - g\partial F_q/\partial p = 0 \quad (2b)$$

where N is the net outgoing radiation flux, C_pF_θ, LF_q are the convective fluxes of liquid water potential temperature and total water. As a simplification, we shall assume constant divergence, D, through the CBL so that ω is linear, and ignore the variation of (T/θ). Integrating (2) through the CBL from surface, p_O, to inversion top, p_T, then gives

$$\omega_T(\theta_T - \bar{\theta}) - (g\overline{\theta/C_pT})\Delta N_T + gF_{O\theta} = 0 \quad (3a)$$

$$\omega_T(q_T - \bar{q}) + gF_{Oq} = 0 \quad (3b)$$

where the overbar denotes a CBL average; ω_T, θ_T and q_T are the subsidence, potential temperature and mixing ratio, respectively, at CBL top; ΔN_T, is the net radiative flux difference across the CBL (typically positive), and $F_{O\theta}$, F_{Oq} are now the surface fluxes.

Since θ and q lie on a mixing line between (θ_{MO}, q_{MO}) and (θ_T, q_T) for both clear and cloudy profiles, the averages $\bar{\theta}$, $\bar{q}$ also lie on this mixing line and can be reexpressed as a linear combination with a coefficient α

$$\bar{\theta} = \theta_{MO} + \alpha(\theta_T - \theta_{MO}) \quad (4a)$$

$$\bar{q} = q_{MO} + \alpha(q_T - q_{MO}). \quad (4b)$$

Given the mixing line, and the specified β, as well as cloud base and cloud top, the coefficient α could be computed in (4a), and (4b), and it is typically ~0.25 for a 30% cloud fraction. However, we do not need to compute α. Substituting (4) in (3) gives

$$\omega_{T'}(\theta_T - \theta_{MO}) - (g\theta/C_pT)\Delta N_T + gF_{O\theta} = 0 \quad (5a)$$

$$\omega_{T'}(q_T - q_{MO}) + gF_{Oq} = 0 \quad (5b)$$

where $\omega_{T'} = (1 - \alpha)\omega_T$ is a modified subsidence. This transformation removes the vertical structure represented by $\theta(p)$, $q(p)$, and gives a vertical divergence term involving a reduced subsidence and only *boundary* values for the CBL. We shall use only $\omega_{T'}$ as a parameter representing subsidence. In essence, our bulk CBL model ignores any changes in the internal structure of the CBL by assuming constant values for β and a constant divergence profile. The mixed layer model is a special case with $\beta = \alpha = 0$ and $\theta_{MO} = \bar{\theta}$. Furthermore, if we had not assumed constant divergence in the CBL, than $\bar{\theta}$, $\bar{q}$ become simply divergence weighted values, and the value of α is typically reduced.

d. Surface flux parameterization

We shall use the bulk aerodynamic formulas to give the surface fluxes

$$F_{O\theta} = \omega_O(\theta_O - \theta_{MO})/g \quad (6a)$$

$$F_{Oq} = \omega_O(q_O - q_{MO})/g \quad (6b)$$

where a surface transfer scale has been defined as

$$\omega_O = \rho_O g C_D V_O \quad (7)$$

where ρ_O, V_O are surface air density and windspeed, and C_D is a surface transfer coefficient. We shall assume saturation at the sea surface temperature (SST) and pressure, so that these give θ_O, and q_O. (θ_{MO}, q_{MO}) are

defined 2 mb above the surface, ω_O, proportional to the surface windspeed will be an important *external* parameter in our analyses. It is, in fact, the only point where atmospheric dynamic processes enter our solutions. $\omega_O = 0.1$ Pa s^{-1} corresponds to $V_O = 6.7$ m s^{-1} with $C_D = 1.3 \times 10^{-3}$.

e. Tropospheric thermodynamic structure

Above the CBL the temperature and moisture profiles are parameterized in a simple way. We assume (following Sarachik 1978) that the deep convection in the ascending branch of Fig. 1 adjusts the tropospheric temperature structure to a moist adiabat. For the coupled solutions the temperature profile follows the moist θ_{es} adiabat through the low level θ_e from CBL top to the tropopause (itself found by the pressure where this θ_{es} adiabat reaches 195 K, the fixed temperature of the lower stratosphere). For the uncoupled CBL solutions, we break the link to the low level θ_e by specifying this moist adiabat. Although a more refined deep convective adjustment scheme could be used to give a thermal structure closer to that observed (e.g., Betts 1986), the moist adiabat is probably satisfactory for *radiative* purposes, because the tropical moisture structure above the CBL is poorly understood (Betts and Albrecht 1987), and we are not modeling upper level clouds.

The moisture profile above the CBL plays an important role. The bulk radiative cooling of the CBL increases sharply as the mixing ratio above the CBL decreases, and moisture at high levels reduces the bulk cooling of the troposphere. This vertical moisture profile was found by interpolating between values at the CBL top and the tropopause. From the mixing ratio q_T, just above the CBL, we computed a corresponding saturation pressure departure $\mathcal{P}_T = (p^* - p)_T$. The moisture at the tropopause was found by specifying $\mathcal{P}_{TR} = (p^* - p)_{TR}$. For most of the studies we set $\mathcal{P}_{TR} = -30$ mb, which corresponds to roughly 10% relative humidity at (typically) 130 mb. The moisture *profile* between CBL top and the tropopause was then computed by imposing a linear profile of $\mathcal{P}$ with pressure, to give a model profile of q which changes smoothly with q_T. For the uncoupled solutions we explore the sensitivity of the CBL equilibrium to the specification of q_T. We then empirically coupled q_T and the tropospheric moisture to the low level θ_e. Betts and Albrecht (1987) noted that the air above the CBL seemed to have subsided on average from a little above the freezing level in the tropical atmosphere. We roughly fitted this by specifying q_T as saturation q_s at -7°C on the tropospheric moist adiabat, θ_{es} (itself equal to the low level θ_e). This couples q_T to θ_{es} so that q_T increases slowly as the troposphere warms (Table 1). Although this increase is small it has a significant radiative impact on CBL top. For the climate experiments in section 5, we shall also show the sensitivity to upper tropospheric moisture represented by $\mathcal{P}_{TR}$.

TABLE 1. Model coupling between moisture at CBL top and tropospheric θ_{es}.

q_T (g kg^{-1})	θ_{es} (K)
4.16	330
4.56	340
4.97	350
5.41	360

f. Radiation model

We estimated radiative fluxes through and above the CBL using the radiation model used in BR. One-dimensional radiative flux computations were made for a clear (unsaturated) atmospheric profile, and for a CBL with "plane-parallel" clouds. Mean radiative fluxes were then found by averaging for a specified CBL cloud fraction. The one-dimensional radiative flux model was based on that used in Harschvardhan et al. 1987. Our primary extension of Harschvardhan et al. (1987) was to treat cloudiness consistently in the solar and longwave computations by using a common liquid water profile derived from the mixing line model discussed in section 2b. Both longwave and solar fluxes are sensitive to cloud fraction, cloud thickness, cloud-top and cloud-base heights. The solar fluxes depend as well on droplet size distribution, which was parameterized following Fouquart (1985), and Stephens (1978).

We computed fluxes and heating and cooling rates every 10 to 700 mb; every 25 mb above up to 50 mb, and at a higher resolution above that. There is a 2 mb surface layer from 1012 to 1010 mb. The longwave model accounts for absorption and emission by water vapor, carbon dioxide, and ozone, and treats clouds as multilayer absorbers which are nearly black, but with single-layer emissivities based on cloud liquid water. The shortwave model includes absorption by water vapor, absorption by ozone above any cloud layer, nonconservative multiple scattering by cloud droplets, and direct and diffuse reflection by the ocean surface. Surface temperature, and surface albedos for scattering of direct and diffuse solar radiation, and the solar zenith angle are specified. A reference ozone mixing ratio profile, and a climatological carbon dioxide concentration (330 ppm) are used except for the doubled CO_2 experiment.

We chose a single solar zenith angle of 51.74° to approximate the daytime incoming shortwave radiation averaged over the tropics (23.3°N to 23.3°S) at either equinox, when the sun is over the equator. This conventional definition of the tropics for this average is clearly a little arbitrary, but uncertainties in fractional cloudiness impact the incoming net shortwave as much as the flexibility in choice of mean zenith angle.

The stratospheric temperature and radiative absorb-

ers were given fixed mean values typical of the tropics. Above the CBL the temperature and moisture structure up to the tropopause were computed as discussed in section 2e. Clear and cloudy CBL profiles were constructed using a mixing line model (section 2b). Only a single cloud thickness was used with base at the LCL of the air nearest the sea surface and top at the last model level below the computed CBL top (which was interpolated between model levels). The model solutions use net flux differences for the subcloud layer, the CBL and the troposphere, and the net flux at the ocean surface; but not the details of the radiative fluxes within the CBL, or upper troposphere. We interpolated the radiative fluxes between model levels to the cloud-base, cloud-top and the tropopause pressures found by the budget model (see 2g and 2h).

g. *Conceptual solution*

The four equations (5a), (5b), (6a) and (6b) appear to have eleven unknowns:

$$F_{O\theta}, F_{Oq}, \theta_T, q_T, \theta_{MO}, q_{MO}, \theta_O, q_O, \omega_{T'}, \omega_O, \Delta N_T.$$

Of these ΔN_T will be computed from the radiation model, and ω_O will always be a specified external parameter, related to the surface wind through (7). Here q_T is specified or modeled as discussed in section (2e); θ_O and q_O are found from the fixed sea surface pressure (1012 mb); and SST, which is either specified (in sections 3 and 4), or determined by a further constraint [see section 2h(3)]. For the uncoupled solutions (section 3), we shall specify $\omega_{T'}$, while for the coupled solutions (sections 4 and 5), this is determined by a tropospheric energy balance constraint [see section 2h(2)]. This leaves five unknowns, θ_{MO} and q_{MO}, which give low level θ_e, the surface fluxes $F_{O\theta}$ and F_{Oq}, and θ_T the free tropospheric potential temperature at the CBL top. One more equation is needed for solution, and we shall introduce a constraint on the surface heat flux [see section 2h(1)].

The CBL top pressure, p_T, does not appear explicitly in the CBL budget equations (5). However, it can be found from θ_T at the CBL top and the tropospheric θ_{es} above the CBL. For the uncoupled solutions, this θ_{es} adiabat is specified (section 2e), while for the coupled solutions, it is linked to the low level θ_e, and we solve

$$\theta_{es}(\theta_T, p_T) = \theta_e(\theta_{MO}, q_{MO}) \tag{8}$$

for p_T. Thus we find from θ_T the equilibrium boundary layer depth, where the radiative cooling is balanced by the surface heat flux, and the subsidence into the CBL of warm air of known θ_{es} from the troposphere above.

h. *Energy balance closures*

1) SUBCLOUD LAYER ENERGY BALANCE

One simple constraint, used by Sarachik (1978), and BR is to specify the surface Bowen ratio

$$b = C_p F_{O\theta}/LF_{Oq} \tag{9}$$

and investigate the sensitivity to b. Measurements over the oceans have shown $b \approx 0.07$ for the undisturbed CBL (Holland and Rasmusson 1973, Pond et al. 1971, Paulson et al. 1972; Augstein et al. 1973). However, sensitivity studies will show (section 3), that the dependence of cloud base and cloud top on b is large, so that the specification of b is a limitation.

In disturbed weather, cooling by subcloud evaporation of rain is known to increase the surface Bowen ratio (Malkus 1962; Augstein 1978; Betts and Simpson 1987), but little is known about its variability in the undisturbed boundary layer. Clearly, however, in equilibrium over a uniform ocean, it is the radiative cooling of the subcloud layer that maintains in air–sea temperature difference, and hence a positive surface heat flux. So we decided to use a simple closure for the surface heat flux, and then to calculate the Bowen ratio b using (9). The equilibrium subcloud layer energy balance (neglecting the subsidence term which is well over an order of magnitude smaller than F_O) is

$$F_{O\theta} - F_{B\theta} + \Delta N_B = 0. \tag{10a}$$

Betts (1973) proposed the closure for the subcloud layer

$$F_{B\theta} = -kF_{O\theta} \quad \text{with} \quad k \approx 0.25; \tag{11}$$

substituting (11) in (10a) gives

$$C_p F_{O\theta} = -\Delta N_B/(1 + k). \tag{10b}$$

This couples the surface heat flux directly to the radiative cooling for the subcloud layer, which we can compute. Observational studies have shown a negative sensible heat flux at cloud base (LeMone and Pennell 1976). However, (11) is not well established for the subcloud layer, (see Appendix) and we can only guess that $0.5 < (1 + k)^{-1} < 1.0$. We decided to use $k = 0.25$ or $(1 + k)^{-1} = 0.8$. Our results are not very sensitive to k (see section 3f). With this closure (10b), the surface heat flux and Bowen ratio [from (9)] decrease with increasing cloud fraction, as the radiative cooling of the subcloud layer decreases.

This link between subcloud layer radiative cooling and the surface sensible heat flux is clearly an important area for future work. However, the detailed coupling of the buoyancy flux, the convective enthalpy flux, cloudiness and the radiative flux within the CBL is beyond this study. Another important area is the testing of radiation models. There is still considerable uncertainty in the magnitude of the longwave cooling of the moist tropical subcloud layer (Cox, personal communication 1988).

2) TROPOSPHERIC ENERGY BALANCE

The atmospheric energy balance averaged over the tropics can be written

$$C_p F_{O\theta} + LF_{Oq} = \Delta N_{TR} + \delta N_{uc} + X_A \tag{12}$$

where ΔN_{TR} is our net radiative flux difference between surface and tropopause, X_A the atmospheric export of energy out of the tropics, and δN_{uc} the perturbation to the radiative flux divergence associated with upper level clouds. We shall neglect upper clouds and the atmospheric export by setting

$$\delta N_{uc} + X_A \approx 0 \tag{13}$$

to give

$$C_p F_{Oq} + L F_{Oq} = \Delta N_{TR}. \tag{14}$$

This is the closed tropical model of Sarachik (1978) and BR. Upper clouds heat the tropics, and the atmospheric export to mid-latitudes cools, so that although the two terms in (13) are each significant, ($\approx$20–30 W m^{-2}, averaged over the tropics: Ramananthan 1987), they are of opposite sign, with the result that (13) is a fair approximation. Clearly, however, (13) is a serious limitation for climate studies.

Equation (14) will be used for the troposphere and ocean coupled solutions to give the effective subsidence $\omega_{T'}$. The method of solution follows BR. We rewrite (5b), and (6b) as

$$gF_{Oq} = \omega_O(q_O - q_{MO}) = \omega_N(q_O - q_T) \tag{15}$$

where

$$\omega_N = \omega_O \omega_{T'}/(\omega_O + \omega_{T'}). \tag{16}$$

This directly links the surface moisture flux to the q difference between surface and free atmosphere (Betts 1983). Then substituting (9) and (14) in (15), we find

$$\omega_N = g\Delta N_{TR}/(1 + b)L(q_O - q_T). \tag{17}$$

This gives the bulk transfer scale, ω_N, [and $\omega_{T'}$ from (16)] from the bulk tropospheric cooling ΔN_{TR}. This computation of ω_N is the crucial step in finding our tropospherically coupled solutions. We then solve (15) for F_{Oq} and q_{MO}. The θ budget can also be expressed in terms of ω_N by rearranging (5a), using (16), to give

$$\begin{aligned} gF_{O\theta} &= \omega_O(\theta_O - \theta_{MO}) \\ &= \omega_N(\theta_O - \theta_T) + (1 - \omega_N/\omega_O)(g\overline{\theta/CpT})\Delta N_T. \end{aligned} \tag{18}$$

Given ω_N from (17), and $F_{O\theta}$ from (10b), (18) can be solved for θ_{MO} and θ_T. Cloud base and the low-level θ_e are found from θ_{MO}, q_{MO}: these give the tropospheric moist adiabat using (8), and hence p_T from θ_T.

3) Oceanic energy balance

For the uncoupled and tropospheric coupled solutions for the CBL we specify SST, but in section 5 we shall present ocean coupled solutions in which SST is determined by the energy balance at the ocean surface. This is a long timescale process: the oceanic circulations and storage can take years to centuries to reach equilibrium. However, the solutions may be of qualitative interest on shorter seasonal timescales (say >100 days).

Energy balance at the sea surface for a tropical ocean can be written

$$N_O - L F_{Oq} - C_p F_{O\theta} = X_O \tag{19}$$

where N_O is the net incoming radiative flux at the surface, and X_O is the mean oceanic export from the tropics (expressed as a mean flux). For a closed tropical ocean we could neglect X_O. For the present climate, X_O is probably $\approx$20 W m^{-2}, at least for the Northern Hemisphere (VonderHaar and Oort 1973), so its neglect would be significant. The longwave component of N_O depends on the surface temperature and atmospheric structure, but the shortwave incoming radiation is primarily controlled by the cloud fraction, which has a high albedo. We are modeling neither cloud fraction nor X_O, so we decided to set both to plausible values (based on observations), in order to give a reasonable mean tropical SST of 300 K for our baseline case. With a cloud fraction of 25% (which, gives a tropical albedo of 26% comparable to that in Stephens et al. 1981) this balance is achieved with X_O = 18 W m^{-2} (see section 5). Substituting (14) in (19) gives

$$N_{TR} = X_O \tag{20}$$

i.e., net incoming radiation at the tropopause equal to the oceanic export. For different surface winds, we varied SST until (20) was satisfied. As a climate model, the assumption of fixed cloud fraction and oceanic export is clearly a limitation; however, over a 6° K change of SST, the surface sensible and latent heat fluxes change by $\approx$30 W m^{-2}, (see sections 4 and 5). Even a 20% change in the value of X_O would be a significantly smaller term.

3. CBL equilibrium: Uncoupled solutions

We shall present results in three sections with an increasingly coupled model representing increasing timescales. In this section we shall present results for the CBL equilibrium for a given SST and given troposphere above the CBL. These represent the equilibrium response of the CBL to diurnally averaged radiative forcing on timescales of the order of a day or two. We call these *uncoupled* solutions because the upper tropospheric temperature and moisture, and subsidence at CBL top will be specified rather than coupled to the low-level θ_e and the tropospheric radiative budget [Eq. (14)]. In the following section 4, we shall show solutions in which the CBL is coupled to the troposphere and constraint (14) is used; in section 5 we shall present the fully coupled solutions in which SST is constrained by the surface radiative budget [Eq. (19)].

For the uncoupled CBL solutions, there are many external variables, and we shall show only the sensitivity to some. We shall take the fully coupled solutions (from section 5) as a reference point and vary parameters

about these values to facilitate comparison between sections. We shall vary sea surface temperature, surface wind speed, tropospheric moisture, and show the sensitivity to Bowen ratio. Table 2 shows the basic parameter set.

Since the radiative fluxes depend on the thermodynamic structure, the method of solution was to iterate the system of equations to convergence. We shall present three key parameters to represent the equilibrium CBL: cloud-base pressure, p_B, and low-level θ_e derived from θ_{MO} and q_{MO}; and cloud-top pressure, p_T, derived from θ_T [from Eq. (5a), knowing this point lies on a tropospheric θ_{es} adiabat above the CBL].

a. CBL structure as a function of SST

Figure 3 shows the dependence of CBL structure, represented by cloud base, cloud top (solid lines) and lowest level θ_e (heavy dashes) on SST, with fixed surface wind speed. For an SST of 300 K typical of the tropical oceans, we obtain an equilibrium cloud base near 950 mb, cloud top (and inversion top) near 800 mb and a low-level θ_e of 347 K. This is in good agreement with the observed mean CBL structure in the tropics. With increasing SST, cloud base barely changes, while the equilibrium cloud top inversion rises rapidly, so that the uncoupled model predicts a deeper CBL over warmer oceans. The steep increase in θ_e with SST is of great importance. It illustrates the tight coupling of the boundary layer to the ocean. Ocean surface θ_{es} (light dashes) also increases with SST, but the subcloud θ_e remains about 14–24° K lower (over this temperature range), corresponding to saturation near 950 mb at the top of the nearly adiabatic subcloud layer.

Figure 3 shows that for a fixed subsidence parameter and fixed upper troposphere, cloud top is quite sensitive to SST. The cloud layer disappears around an SST of 296 K (see dotted extropolation: our model cannot resolve cloud layers $\leq$ 20 mb in depth). This is a greater sensitivity than shown by Albrecht et al. (1979), who specified constant divergence, so that as CBL top increases, ω_T does also. These equilibrium solutions satisfy only the CBL energy balance constraints. The tropical upper troposphere has a fixed temperature structure on the θ_{es} = 347 K moist adiabat, corresponding to the low level θ_e from the fully coupled solution with an SST = 300 K.

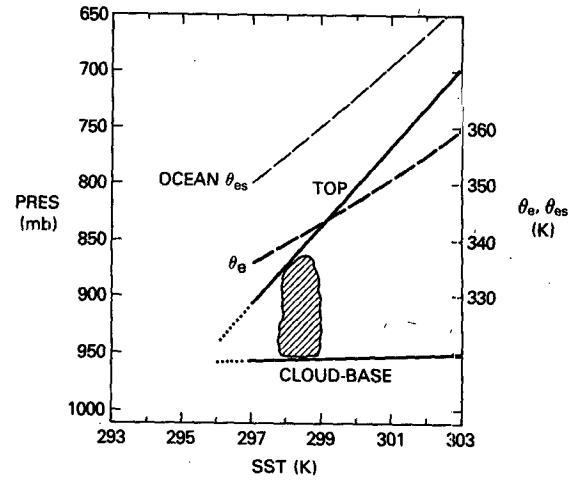

FIG. 3. Uncoupled CBL solutions for cloud base and CBL top (solid lines) and low-level θ_e (long heavy dashes: scale on right) as a function of SST, for surface wind parameter ω_O = 0.1. θ_{es} for the sea surface is shown as long light dashes.

TABLE 2. Model parameters: Base set.

Solar zenith angle	51.74°
Surface albedo	0.07
Incoming SW flux	1360.3 W m^{-2}
CBL parameters	
cloud	β_c = 0 (subcloud); 0.6 (cloud layer)
environment	β_u = 0.2 (subcloud); 1.2 (cloud layer)
Subcloud layer closure parameter	k = 0.25
Tropopause subsaturation	$\mathcal{P}_{TR}$ = −30 mb
Mixing ratio just above CBL	q_T = 4.8 g kg^{-1}
Ocean surface temperature	SST = 300 K
Surface wind parameter	ω_O = 0.1 Pa s^{-1} (≡6.7 m s^{-1})
Tropospheric	θ_{es} = 347 K
Subsidence parameter	$\omega_{T'}$ = 0.05 Pa s^{-1}
Cloud fraction	= 25%

Figure 3 suggests that if the SST is above 300 K, then the CBL equilibrium will give $\theta_e >$ 347 K, sufficient to give deep convective instability. The relationship between tropical SST and deep convection was noted by Gadgil et al. (1984). Recent studies of tropical convection (Graham and Barnett 1987) have shown that there is a sharp change in convection regimes above a critical SST, T_c, which is about 27.5°C for much of the Indian and Pacific oceans, and somewhat lower (<27°C) for the Atlantic. They found that deep convection requires an SST above this threshold, while below it, only shallow CBL clouds are typically observed. Figure 3 suggests a simple explanation of this: θ_{es} for the deep troposphere and the low level capping inversion is typically in the range 347–350 K in the tropics. Our equilibrium CBL θ_e reaches 347 K for an SST of 27°C and 350 K for an SST of 27.7°C. This also suggests that the reason for the well-known threshold for hurricane formation *only* at SSTs > 26.5°C (299.7 K) (Palmen 1948) is directly related as well to the boundary layer equilibrium θ_e, which for larger SSTs exceeds the mean θ_{es} of the deep tropical atmosphere.

Figure 4 shows the increase in the equilibrium surface sensible and latent fluxes (solid lines) with SST. The sensible heat flux increases +0.6 W m^{-2} K^{-1}, and the latent heat flux by +11.7 W m^{-2} K^{-1}, as SST increases. There is little change in the surface Bowen ratio (long dashes) of ~0.06. This rate of increase of

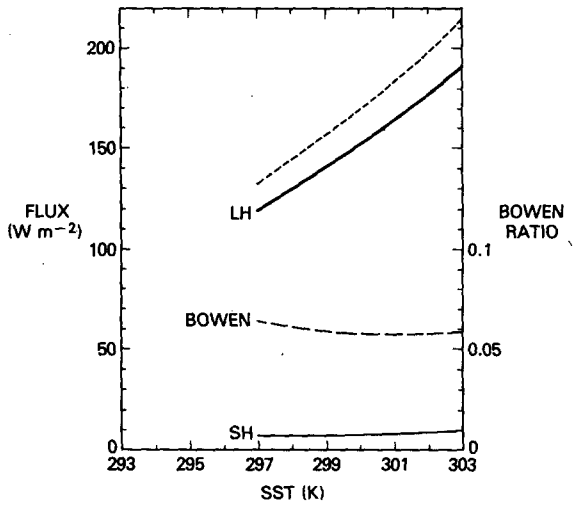

FIG. 4. Surface sensible and latent heat fluxes (solid lines) and Bowen ratio (long dashes) for uncoupled CBL solutions as a function of SST, for $\omega_O = 0.1$. The latent heat flux for a higher wind speed ($\omega_O = 0.15$, approximately 10 m s^{-1}) is shown as short dashes.

the total surface heat flux with SST is double that of the tropospherically coupled CBL discussed in section 4. For comparison, a simple ocean–atmosphere interaction model which *assumes* constant relative humidity (of 73.8%) and wind speed has a slope of latent heat flux of 9.2 W m^{-2} K^{-1} near 300 K. The short dashed line on Fig. 4 shows latent heat flux with SST for a higher wind speed ($\omega_O = 0.15$ Pa s^{-1}).

b. *The effect of surface wind speed*

We then kept SST fixed at 300 K and varied surface wind speed. Figure 5 shows that with increasing wind speed, cloud base descends, and cloud top rises to give a deeper CBL. As surface wind falls, the subcloud layer cools and dries in response to the subsidence above, and the cloud layer gets thinner, until at low wind speeds ~ 3 m s^{-1}, it is no longer possible to maintain an equilibrium cloudy boundary layer; θ_e increases with wind speed, rapidly at low wind speeds, with a more asymptotic behavior at higher wind speeds towards the θ_{es} of the ocean (365 K at an SST of 300 K, shown as long light dashes). This equilibrium suggests that regions of climatically higher wind speed should have climatically higher θ_e, and more deep convection. It also confirms that in the equilibrium hurricane (Emanuel 1988a, 1988b), the increase in surface wind will tend to drive the CBL to higher θ_e.

Figure 6 shows the response of the surface fluxes to surface wind changes as the boundary layer structure adjusts. With increasing wind, the latent heat flux increases and the sensible heat flux decreases (as the air–sea temperature difference becomes very small: Fig. 7), and correspondingly the Bowen ratio falls. The sea–air Δq difference also falls rapidly with increasing wind speed, (Fig 7) so that the increase in the LH flux with ω_O is *much less steep* than if Δq or relative humidity remained constant. The dotted line in Fig. 6 indicates for comparison the linear change of latent heat flux with ω_O, for constant Δq, corresponding to the values at $\omega_O = 0.1$. In sections 4 and 5, we shall show that the coupled solutions have even less of an increase with wind speed.

c. *Impact of tropospheric moisture above CBL*

Figure 8 shows the dependence on q_T, the mixing ratio just above the CBL at the inversion top. The

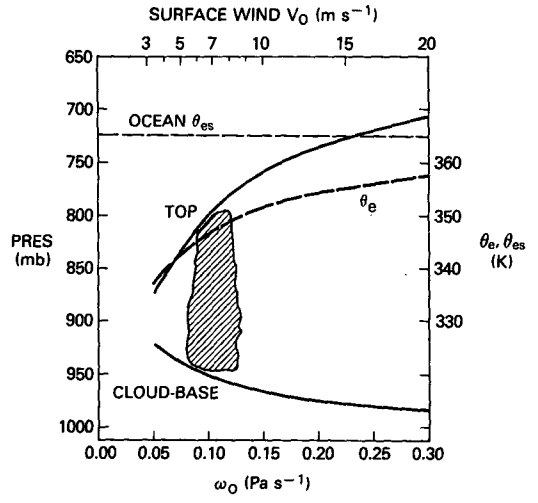

FIG. 5. As in Fig. 3 but for fixed SST = 300 K as a function of surface wind. Ocean θ_{es} shown as long light dashes.

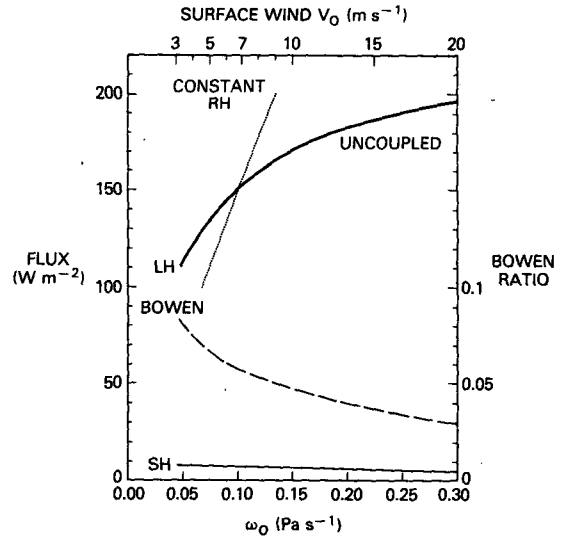

FIG. 6. As Fig. 4 but as a function of surface wind parameter ω_O. Dotted line shows the slope of latent heat flux with surface wind for fixed relative humidity.

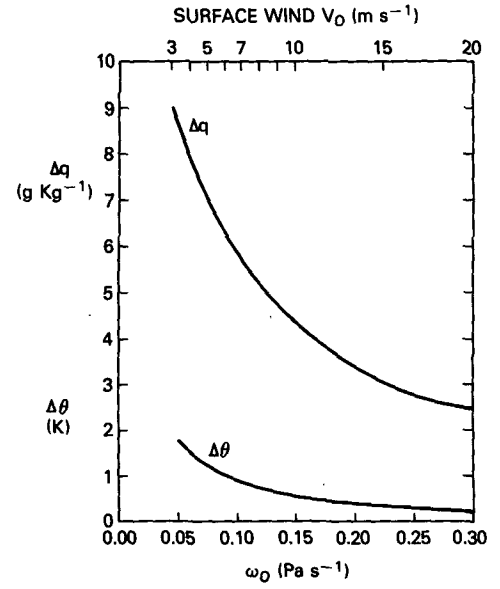

FIG. 7. Sea–air difference of mixing ratio (Δq) and potential temperature ($\Delta\theta$) as a function of surface wind for uncoupled equilibrium solutions.

model interpolates the moisture structure from p_T to a specified moisture at the tropopause (section 2e), so that increasing q_T primarily increases the moisture above the CBL in the lower and middle troposphere. There is an impact on cloud-base and low-level θ_e, as the subcloud layer moistens. The impact on cloud top is larger: this comes down as q_T increases. This is because the net radiative cooling of the CBL is reduced if there is moister air above, and this cooling is an important control on the equilibrium height of the cloud top inversion [see Eq. (5a)].

In this uncoupled solution with fixed subsidence, the CBL also moistens as q_T increases. This reduces the change in the radiative cooling of the CBL, and damps the response of cloud top. The moister CBL reduces the surface latent heat flux. We shall find in section 4a that the response of the tropospherically coupled CBL is significantly different (Fig. 12). Conventional wisdom, observing that deeper boundary layers had drier air above, might ascribe this to the usual decrease of q with height. This result suggests that the connection is the reverse. Dry air above the CBL will lead to stronger radiative cooling and a deeper equilibrium height. This focuses attention on the origin of the air near 700 mb above the CBL. Betts and Albrecht (1987) in a study of the CBL over the equational Pacific noted that it appeared that the air entering the top of the CBL, with typically $2 < q < 6$ g kg^{-1}, had sunk, not from a cumulonimbus outflow level near 200 mb, but only from near the freezing level: over a period of 6 days at 40 mb day^{-1}, the radiatively driven subsidence rate. They noted that the origin of the air entering the top of the CBL deserved further study, because of its impact on the CBL structure. Figure 8 confirms that one major impact is on boundary layer depth.

d. *Impact of surface Bowen ratio*

As a sensitivity study, we replaced the subcloud layer closure (10b) which determines the surface sensible heat flux, with a specified Bowen ratio, b, so that

$$C_p F_{O\theta} = bLF_{Oq} \tag{9}$$

Figure 9 shows that cloud base and cloud top decrease sharply with increasing Bowen ratio. Cloud base falls because increasing Bowen ratio, at fixed SST and subsidence, means a cooler subcloud layer. The radiative

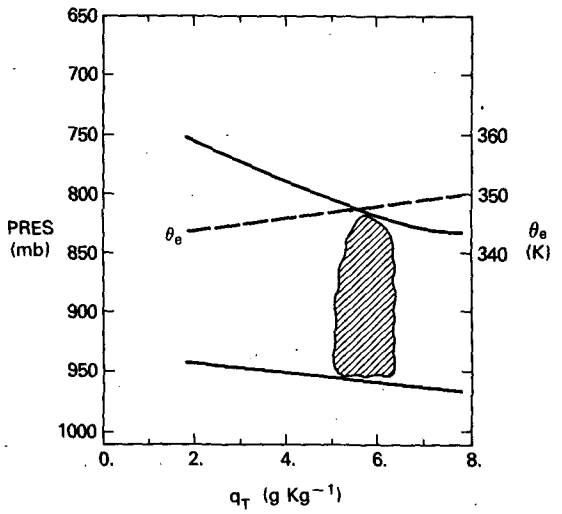

FIG. 8. As in Fig. 3 except as a function of mixing ratio above inversion.

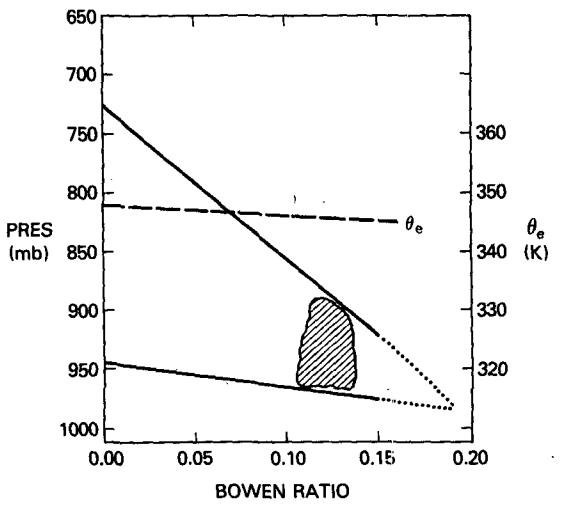

FIG. 9. As in Fig. 3 except as a function of specified surface Bowen ratio.

cooling in (5a) must now balance an increased sensible heat flux, and cloud top must fall to reduce the subsidence warming term. The cloud layer disappears around a Bowen ratio of 0.18 (dotted extrapolation). The low-level θ_e falls a little as θ_{MO} falls.

This result is at first sight only of academic interest, because a Bowen ratio of, say, 0.18 represents a tripling of the surface sensible heat flux to ~25 W m^{-2}. This is much larger than the radiative cooling of the subcloud layer, and cannot be maintained without other cooling processes below cloud base, such as the evaporation of precipitation, which is not included in this model. However, Fig. 9 can, therefore, be regarded qualitatively as the response to the early onset of precipitation. Evaporation below cloud base will increase the Bowen ratio (lowering cloud base) and will reduce the evaporative cooling at cloud top, which in equilibrium gives a lower and weaker inversion. This remains qualitatively true for cloud top, even when precipitation reaches the ground, provided the surface Bowen ratio is then interpreted at the ratio of the liquid water potential temperature (θ_l) flux to the total water (q_t) flux. (However, the surface θ_l and q_t fluxes will then no longer exactly satisfy (6), so extensions of the model are needed.) This response of cloud top to Bowen ratio may also account in part for the uniformity of CBL height over the oceans. The onset of precipitation occurs in some clouds once the CBL top rises much above 800 mb (Byers and Hall 1955; Ludlam 1980; Betts and Albrecht 1987). The onset of precipitation in deeper boundary layers will increase the surface Bowen ratio, and Fig. 9 suggests this will then lower cloud top.

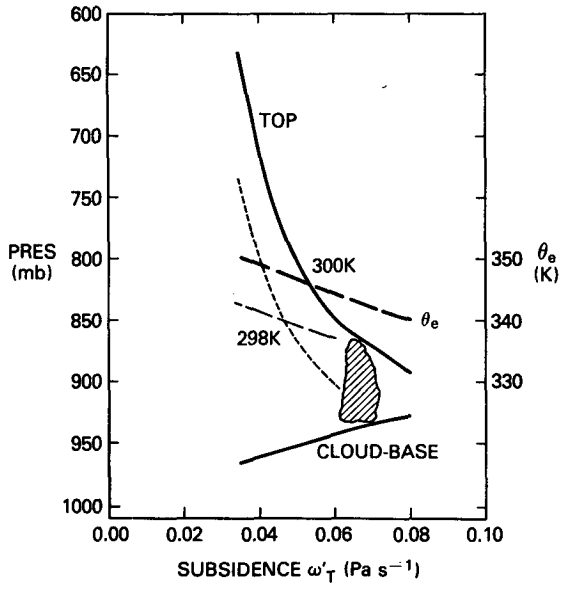

FIG. 10. As Fig. 3 except as a function of specified CBL top subsidence parameter, $\omega_{T'}$. CBL top for a lower SST = 298 K shown dashed, with corresponding θ_e as long light dashes.

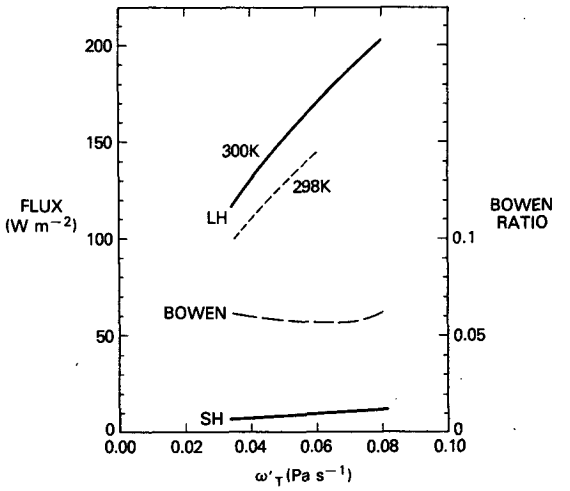

FIG. 11. As Fig. 4 except as a function of CBL top subsidence for SST = 300 K. Latent heat flux for SST = 298 K shown as short dashes.

e. Response of CBL to variations in subsidence

Figure 10 shows the variation in CBL parameters with the subsidence parameter, $\omega_{T'}$, for SST = 298 K (light dashes) and 300 K (heavy). The tropospheric radiative equilibrium solution (see section 4) corresponds to $\omega_{T'} = 0.05$. For smaller $\omega_{T'} < 0.05$, the CBL rapidly deepens, and by $\omega_{T'} = 0.035$ the CBL has become unrealistically deep, and the low level θ_e, which increases with decreasing subsidence, has reached 350 K, above the θ_{es} = 347 K of the deep troposphere. Conversely, as $\omega_{T'}$ increases, θ_e decreases as the CBL dries, cloud base rises, and cloud top descends; and by $\omega_{T'} = 0.085$ Pa s^{-1}, the layer becomes cloud free and this model breaks down.

The fact that we observe a CBL top near 800 mb over most of the tropical oceans (Betts and Albrecht 1987) suggests therefore that the subsidence is usually not far from its radiative equilibrium value. Figure 11 shows the response of the surface fluxes to increasing subsidence. The latent heat flux increases rapidly as the increased subsidence dries the CBL. The sensible heat flux also increases for a more indirect reason. The drying of the subcloud layer raises cloud base; which increases the radiative flux divergence of the subcloud layer, so that the subcloud layer cools to increase the sensible heat flux to satisfy (6a) and (10b). The Bowen ratio changes very little.

Figures 10 and 11 show important responses of the CBL to changes in the overlying subsidence. Higher subsidence, typical of the subtropical highs, (as examples) or the subsidence around a hurricane, increases the surface fluxes by lowering CBL θ_e. With lower subsidence than the radiative equilibrium value, the surface fluxes fall, but the low level θ_e rises and the CBL deepens rapidly and deep convection may result.

However, a more complete analysis requires the inclusion of horizontal advection which can modify the heat and moisture balance of the CBL in a different way than simple subsidence.

f. Discussion of uncoupled CBL solutions

The solutions given by Figs. 3–12 can be qualitatively combined to estimate the effect of changes in combinations of parameters. For example, increasing ω_O from 0.1 to 0.15 in Fig. 3 (V_O from 6.7 to 10 m s^{-1}) lowers the cloud base line about 15 mb, lifts the cloud-top line about 40 mb and increases θ_e about 5° K, roughly independently of SST. The corresponding latent heat flux curve is shown (short dashes) in Fig. 4. This change with wind speed is basically the same as shown in Figs. 5 and 6 at one SST. Figures 10 and 11 show as dotted lines cloud top, θ_e and latent heat flux for a lower SST = 298 K [cloud base is essentially unchanged (see Fig. 3)].

The change in CBL equilibrium with tropospheric θ_{es} is not shown. Only cloud top is affected; it drops 40 mb as θ_{es} increases from 345 to 351 K. The effect of the closure parameter k in Eq. (11) is small. Changing k from 0 to 0.5 changes the Bowen ratio from 0.07 to 0.05 with the correspondingly small changes in CBL parameters shown in Fig. 9. The main effect of changing cloud fraction is also to reduce the surface Bowen ratio towards zero as cloud fraction increases toward 100%, and the cooling of the subcloud layer falls toward zero.

TABLE 3. Model solution for SST = 300 K, and 25% cloud fraction.

Input parameters	
p_O	1012 mb
SST	300 K
ω_O	0.1 Pa s^{-1}
Cloud fraction	25%
$\mathcal{P}_{TR}$	−30 mb
Model solution	
p_B	954 mb
p_T	796 mb
θ_e	346.8 K
$\theta_O - \theta_{MO}$	0.84 K
$q_O - q_{MO}$	5.9 g kg^{-1}
RH	74%
$F_{OCp\theta}$	9 W m^{-2}
F_{OLq}	150 W m^{-2}
Bowen ratio	0.06
$\omega_{T'}$	0.049 Pa s^{-1}
ω_N	0.033 Pa s^{-1}
θ_T	307.0 K
q_T	4.8 g kg^{-1}
θ_{eT}	322 K
ΔN_B	11 W m^{-2}
ΔN_T	52 W m^{-2}
ΔN_{TR}	158 W m^{-2}

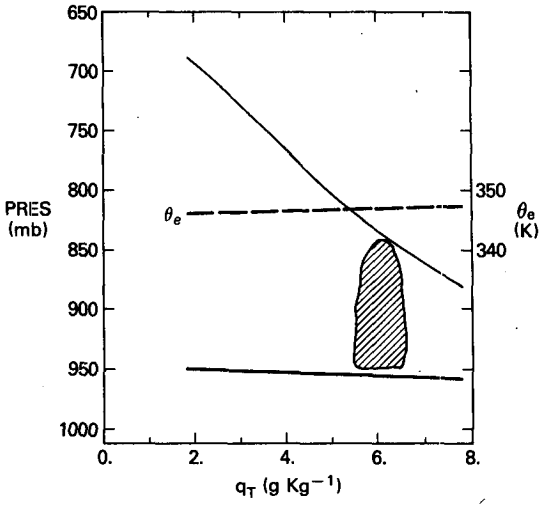

FIG. 12. As Fig. 8 except for coupled tropospheric θ_{es} and CBL top subsidence.

4. Coupled solutions satisfying tropospheric energy balance

We now explore how the CBL equilibrium is altered by introducing constraint (14) for tropospheric energy balance, as well as a tropospheric moist adiabat linked to the low level θ_e. We shall separately couple the moisture, q_T, above the CBL to the low level θ_e, as in Table 1.

a. Basic solution with coupled troposphere

Our steady-state model solution for a tropical mean SST of 300 K with a coupled troposphere is given in Table 3. The values for cloud base near 950 mb, cloud top near 800 mb, low-level θ_e near 347 K and surface sensible and latent heat fluxes of 9 and 150 W m^{-2}, respectively, are quite close to observed climatic values (Holland and Rasmussen 1973; Betts and Albrecht 1987). This gives us confidence in both the basic model structure and assumptions, and in the radiation code.

b. Sensitivity to troposphere moisture

Figure 12 shows the response of the coupled CBL to changing q_T: The moisture at CBL top shows important differences from Fig. 8 for the uncoupled CBL. The change of cloud base and low-level θ_e with increasing q_T is considerably reduced, whereas the fall of cloud top is greatly amplified. This is because ω_N (and $\omega_{T'}$) increases as ($q_O - q_T$) decreases in Eq. (17), despite a small fall in the tropospheric radiation cooling, ΔN_{TR}. Figure 12 shows that the primary effect of coupling q_T to the low level θ_e (Table 1) will be on cloud top, with little impact on cloud base or low level θ_e. In particular, the rise of q_T with θ_e (Table 1) will reduce the rise of cloud top.

The impact of changing the moisture at the tropopause (through $\mathcal{P}_{TR}$) is smaller but quite different. As $\mathcal{P}_{TR}$ increases from −40 to 0 mb (corresponding to a relative humidity change from 5 to 100%) the CBL *deepens* by about 10 mb and θ_e increases +0.8 K as the troposphere radiative cooling decreases by about 7 W m^{-2} (reducing ω_N). This radiative impact of increased moisture at the tropopause is much more significant in the ocean coupled solution discussed in section 5.

c. *Sensitivity to SST*

Figure 13 shows the dependence of CBL structure, represented by cloud base, cloud top and lowest level θ_e over a 10° K range of SST for the tropospherically coupled system. With increasing SST, cloud base now falls steadily while the equilibrium cloud-top inversion rises (solid lines). Three cloud-top curves are shown. The solid line (labeled coupled), which shows the slowest CBL deepening with increasing SST, is for the fully coupled troposphere with the moist adiabat θ_{es}, and moisture q_T both coupled to the low level θ_e, and the subsidence coupled to the tropospheric cooling through (17) and (16). The dashed line has q_T fixed at 4.8 g kg^{-1}, but coupled subsidence and temperature (moist adiabat θ_{es} = low level θ_e), and the dotted line is the steep rise of cloud top with SST for the uncoupled solutions (from Fig. 3). We see that, with greater coupling, the CBL depth changes more slowly with SST. With a coupled troposphere the cloud top subsidence actually decreases with increasing SST, because ($q_O - q_T$) increases faster than ΔN_{TR} in (17). However, cloud top θ_T increases so rapidly with θ_{es}, (at constant p_T), that the cloud top rise is reduced. The coupling of q_T to the low level θ_e further reduces the rise of cloud top, but has virtually no effect on cloud base or θ_e, as discussed in section 4b.

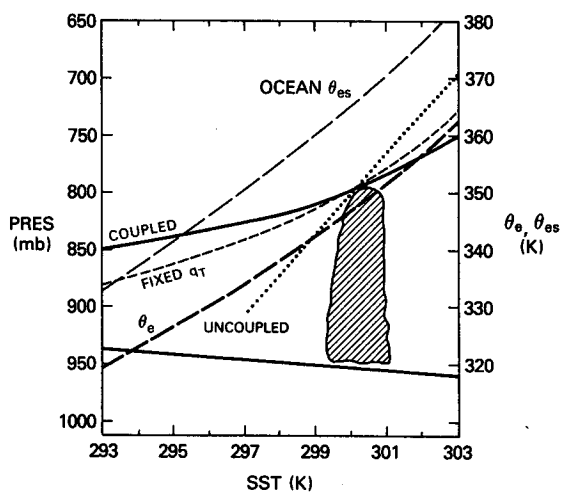

FIG. 13. As Fig. 3 except for coupled tropospheric θ_{es}, q_T and subsidence: cloud base and CBL top as solid lines, θ_e as heavy dashed lines. Short dashes show cloud top for fixed q_T, but coupled θ_{es} and subsidence. Dotted line is CBL top for uncoupled solution from Fig. 3.

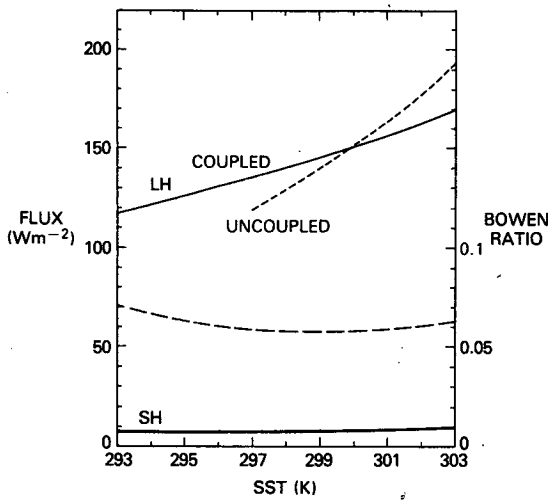

FIG. 14. As Fig. 4 except for tropospherically coupled solution. Short dashed line is latent heat flux from Fig. 4.

The rise of θ_e (heavy dashes) with SST is a little steeper than the uncoupled solution in Fig. 3. The coupling of the boundary layer to the ocean is a little tighter: with the CBL θ_e ranging from 14–21° K below the θ_{es} of the ocean (long light dashes) over the SST range from 293–303 K. Over the whole range of SST, the vertical gradient of θ_e (not shown) between the subcloud-layer and the air above the inversion satisfies the cloud-top entrainment instability criteria (Randall 1980; Deardorff 1980; Betts 1983). This is consistent with our assumed small fraction of cumulus clouds.

The corresponding wet-bulb depression at the surface varies very weakly with SST. A simple formula for the atmospheric low level T_{wO} (at this wind speed 6.7 m s^{-1}) is

$$T_{wO} = T_O - 3.6[1 + 0.008(300 - T_O)]. \quad (21)$$

The low level equilibrium θ_e [saturation at (p_O, T_{wO})] can be found from Eq. (21) to an accuracy of ~0.2° K for 293 < T_O < 303 K.

Figure 14 shows the increase in the equilibrium surface sensible and latent fluxes with SST for the fully coupled solution (solid lines). For 297 < SST < 303 K the sensible heat flux increases +0.5 W m^{-2} K^{-1}, and the latent heat flux by +5.6 W m^{-2} K^{-1}. The surface Bowen ratio changes weakly with SST. This rate of increase of the latent heat flux with SST is about half that of the uncoupled CBL, shown dashed (from Fig. 4). The rate of increase in the total surface heat flux is now almost identical to the rate of increase in the surface emittance given by differentiating Planck's law.

$$\partial E/\partial T = 4\sigma T^3$$
$$= 6.1 \text{ W m}^{-2} \text{ K}^{-1} \quad \text{at} \quad 300 \text{ K}.$$

This presumably reflects the tight coupling to the SST of the CBL structure and the radiative emission to space.

d. Sensitivity to surface wind speed

Figure 15 shows that with increasing wind speed, cloud base descends, and cloud top rises to give a deeper CBL. Three cloud-top curves are again shown. The solid line for tropospherically coupled subsidence, θ_{es} and q_T, again shows the least variation with surface wind speed (cf. Fig. 13); the short dashed line with q_T fixed (but coupled subsidence and θ_{es}) shows more deepening of the CBL with wind speed, and the dotted curve for the uncoupled solutions (from Fig. 5) shows the sharpest slope of cloud-top pressure with wind speed. Once again the increase in cloud-top θ_T associated with rising θ_{es} dominates over a weak decrease in cloud-top subsidence in Eq. (5a), so that the rise of cloud top with surface wind is reduced for a coupled tropospheric temperature and subsidence. The coupling of q_T to θ_e further reduces the deepening of the CBL, as discussed in section 4b.

There is a singularity at low wind speeds $\sim$3 m s^{-1}, where it is no longer possible to maintain an equilibrium cloudy boundary layer. As surface wind falls, the subcloud cools and dries in response to the subsidence above, and the cloud layer gets thinner. The change of θ_e with wind speed is similar to the uncoupled solution in Fig. 5; θ_e increases with wind speed rapidly at low wind speeds and with a more asymptotic behavior at

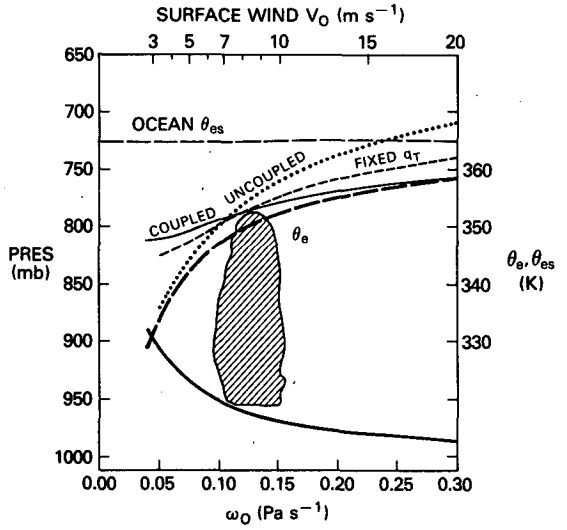

FIG. 15. As Fig. 5 except for tropospheric coupled solution. Solid lines are for coupled θ_{es}, q_T and subsidence; short dashed line is for fixed q_T, but coupled θ_{es} and subsidence; and dotted line is CBL top for uncoupled solution from Fig. 5.

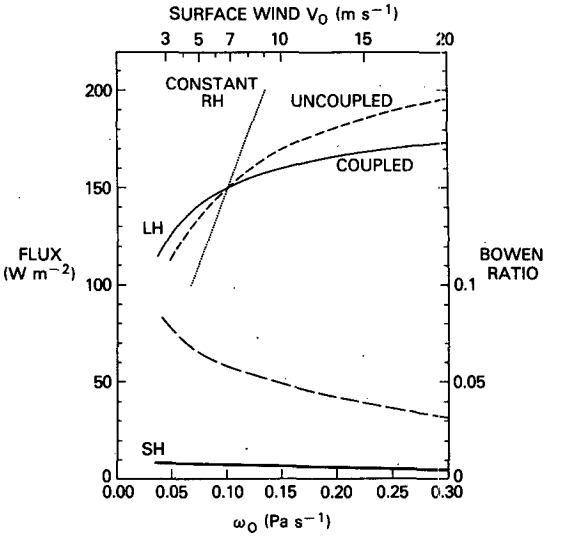

FIG. 16. As in Fig. 6 except for tropospheric coupled solution; compared with uncoupled solution (short dashes), and constant relative humidity solution (dotted).

higher wind speeds towards the θ_{es} of the ocean (light long dashes). This equilibrium again suggests that regions of climatically higher wind speed should have climatically higher low-level θ_e. This could be tested using climatic datasets.

Figure 16 shows the response of the surface fluxes to surface wind changes (solid lines) with coupled θ_{es}, q_T and subsidence. With increasing surface wind, latent heat increases and the sensible heat flux decreases (as the air–sea temperature difference falls), and correspondingly the Bowen ratio (long dashes) falls as in Figure 6. The sea–air Δq difference (not shown) falls more rapidly with increasing wind speed than in Fig. 7 for the uncoupled CBL, so that the increase in the LH flux with ω_O is less than for the uncoupled solution; shown dashed (from Fig. 6). The dotted line again indicates the change with ω_O, for constant Δq corresponding to the values at $\omega_O = 0.1$. We see that with increasing coupling the rise of LH with wind speed becomes much less steep.

e. Tropopause height

The coupled solutions give almost trivially the pressure of the tropopause where the θ_{es} moist adiabat reaches 195 K, the fixed temperature of the lower stratosphere (as in Sarachik 1978). The tropopause pressure falls from 177 to 115 mb as SST increases from 293 to 303 K (θ_e increasing from 320 to 361 K). The change with increasing windspeed is similar.

f. Discussion of tropospheric coupled solutions

We have seen that the introduction of tropospheric coupling has two significant impacts on the CBL struc-

ture and fluxes. One is to reduce the deepening of the CBL with increasing SST and surface wind. This effect is dominated by two processes: first, the increase of cloud-top θ_{es} and q_T with low level θ_e; second, the reduction of the increase of the surface latent heat flux with SST and wind speed. This is caused by changes in the bulk transfer parameter ω_N given by (17). The surface Bowen ratio changes only weakly with SST, but falls rapidly with increasing wind speed, as the CBL adjusts to a lower cloud base as the subcloud layer moistens. We have not shown the coupled CBL response to changing Bowen ratio. Cloud base still falls with increasing Bowen ratio as in Fig. 9, but θ_e is almost constant, and the fall of cloud top is significantly reduced because ω_N falls in (17) as b increases.

g. *Relationship of θ_e to SST and windspeed*

One generalization of our equilibrium results that could be tested with climatic data is that θ_e in the CBL (at, say, 10 m above the ocean surface) is closely related to SST and surface wind speed on climatic timescales. A simple relationship is in terms of the wet-bulb depression of the air near the surface. The weak dependence on SST is given by (21). There is an approximate inverse dependence on wind speed (Fig. 15), so that (21) can be extended to

$$T_{wO} \approx T_O - 0.36[1 + 0.008(300 - T_O)]/\omega_O$$
$$\approx T_O - 24[1 + 0.008(300 - T_O)]/V_O. \quad (22)$$

This gives low level θ_e to <1° K for $5 < V_O < 20$ m s^{-1} and $293 < T_O < 303$ K. A similar approximation for the pressure of cloud base (in mb) is

$$p_B \approx p_O - 5.8[1 + 0.035(300 - T_O)]/\omega_O$$
$$\approx p_O - 390[1 + 0.035(300 - T_O)]/V_O. \quad (23)$$

This fits the cloud-base pressure given by the model to <5 mb over the same range of SST and surface wind speed. The uncoupled solutions in section 3 can be roughly fitted with similar formulae with different temperature coefficients of opposite sign. Note, however, that these relationships ignore the effect of horizontal advection over, say, a warmer ocean.

h. *Relationship of CBL depth to SST*

Figure 13 shows how the increase in CBL depth with increasing SST is reduced by greater tropospheric coupling. An earlier model by Albrecht (1984), which specified divergence and CBL radiative cooling, gave a slope of CBL depth with SST intermediate between our uncoupled and partially coupled solutions (dotted and short dashed lines in Fig. 13). In an observational study along downstream trajectories in the eastern North Pacific towards Hawaii (Neiburger 1960), the observed mean slope and height of the inversion base agrees well with the coupled solution for CBL top (solid line in Fig. 13). His inversion top is, however, 30–40 mb higher. Although our model was constructed for a "global tropics,"and does not include the lag associated with horizontal advection over a warmer SST, it represents solutions for any large region of the tropics for which the energy balance closure (14) is approximately satisfied. It seems likely that the rise of mean inversion height along the NE Pacific trade wind trajectory described by Riehl et al. (1951), Malkus (1956) and Neiburger (1960) is primarily due to the rise in SST. This climatic relationship between CBL top and SST predicted by Fig. 13 clearly deserves further study.

i. *Relationship of CBL depth to radiative cooling*

The CBL top is coupled to the cooling of the CBL through Eq. (5a), which determines θ_T on the upper moist adiabat.

$$\omega_T(\theta_T - \theta_M) = \Delta N_T - F_O. \quad (5a)$$

However, further simplifications are elusive because of the dependence of ΔN_T on the temperature and moisture structure, and ω_T on $\Delta N/(q_O - q_T)$ and ω_O. For example, if we consider the uncoupled CBL, we could approximately relate θ_T to CBL top, p_T by defining a mean lapse rate, Γ

$$\theta_T = \theta_{OO} + \Gamma(p_O - p_T). \quad (24)$$

This gives CBL depth

$$(p_O - p_T)$$
$$= [(\Delta N_T - F_{O\theta})/\omega_T + (\theta_{MO} - \theta_{OO})]/\Gamma. \quad (25)$$

We see that for fixed ω_T, θ_{OO}, Γ, and $F_{O\theta}$, CBL depth increases with ΔN_T and θ_{MO}. If we change only q_T, then ΔN_T increases as q_T decreases, and the q difference between the moist CBL and dry air above increases. If we change SST, then θ_{MO} increases and q_{MO} increases as well; both increasing ΔN_T as the CBL becomes warmer and moister. However, as we consider the atmospherically coupled system, ω_T decreases with SST as $\Delta N_{TR}/(q_O - q_T)$ decreases (both ΔN_{TR} and $(q_O - q_T)$ increase), and Γ increases as θ_e increases. The increase of Γ is sufficient to reduce the dependence of p_T on SST, when compared with the uncoupled CBL. As we couple q_T to θ_e and change ω_O, the complexity of the interaction between the radiation field and the thermodynamic structure increases. It becomes clear why a simple CBL model with N, ω, or q specified is completely inadequate to explain CBL depth and structure over the oceans.

j. *Tropospheric subsidence*

The subsidence parameter, $\omega_{T'}$, at CBL top *decreases* with increasing SST and surface wind. As surface wind increases from 3 to 20 m s^{-1}, and SST from 293 to 303 K, $\omega_{T'}$ decreases from 0.065 to 0.045 Pa s^{-1}, and from 0.074 to 0.044 Pa s^{-1} respectively. This

can be understood as a response to increasing surface forcing: the surface moisture flux increases and a new balance is achieved in (5b), (6b), (15) and (17) with an increase in q_{MO} and ΔN_{TR} (the net cooling to space) and a decrease of $\omega_{T'}$.

5. Coupled sea surface temperature

In section 3, we discussed CBL equilibrium on short timescales ($\approx$day) with a fixed upper troposphere and specified subsidence. In section 4, we coupled the tropospheric thermodynamic structure above the CBL to the low level θ_e, and introduced constraint (14) to determine the effective subsidence at CBL top from the tropospheric energy balance: a timescale of order 10 days. We now introduce the additional constraint (20), related to the oceanic energy balance (19), to determine the equilibrium SST and CBL structure on longer timescales (>100 days).

a. *Cloud fraction and oceanic export*

Neither boundary layer cloud fraction nor the oceanic export (X_O) of energy from the tropics is determined by the model, and both are critical to the determination of ocean equilibrium temperature. Hence we specified reasonable values, consistent with observations, which gave a model equilibrium SST of 300 K, a reasonable value for the tropical mean state. We then did sensitivity studies about this state with fixed cloud fraction and oceanic export, X_O. Our ocean surface albedo is specified at 0.07; the top of the atmosphere (TOA) albedo for the clear sky is ~0.105, and for a plane parallel CBL cloud, it is typically ~0.70. We chose a CBL cloud fraction of 25% to give a TOA albedo of ~25.5% corresponding roughly to an observed tropical mean (Stephens et al. 1981; Ramanathan 1987). For an SST of 300 K and a tropopause subsaturation $\mathcal{P}_{TR} = -30$ mb, this gave a net downward flux at the tropopause (equal to a net ocean source with no atmospheric export) of 18 W m^{-2}: a reasonable value (VonderHaar and Oort 1973). We then set the oceanic export X_O = 18 W m^{-2}, so that the coupled base line model had an equilibrium SST of 300 K.

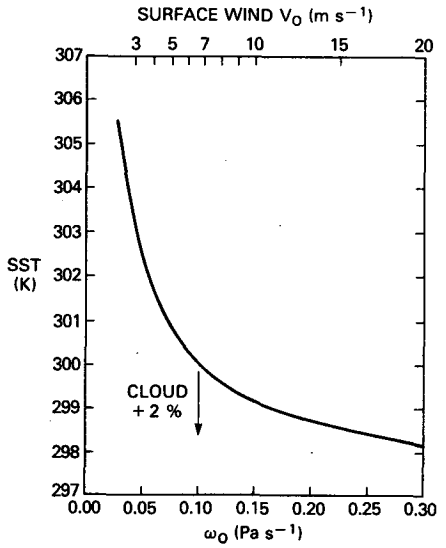

FIG. 17. Change of SST with surface wind for coupled ocean and troposphere.

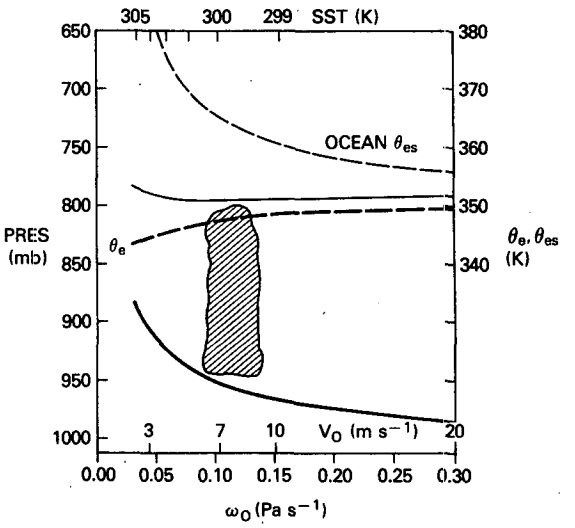

FIG. 18. As in Fig. 5 but for coupled SST and troposphere.

b. *SST as a function of surface wind speed, and cloudiness*

Figure 17 shows the variation in SST as a function of surface wind speed and CBL cloud fraction. For fixed cloud fraction, the equilibrium SST decreases in a nonlinear fashion, with increasing surface wind. As wind speed increases, the increased forcing of the surface evaporation moistens the CBL, and increases the LW radiative cooling to space so that the equilibrium SST falls. Conversely, at low wind speeds, the CBL dries rapidly (section 3b), the cooling to space falls, and SST increases sharply. With a 25% cloud fraction, an oceanic export, X_O = 18 W m^{-1}, and a surface wind of 6.7 m s^{-1} (ω_O = 0.1) the model gives an equilibrium SST of 300 K, close to the observed tropical mean.

This equilibrium SST is very sensitive to cloud fraction because this reflects part of the incoming shortwave radiation. A 2% increase of cloud reduces the SST by 1.5° K at 300 K, as shown on Fig. 17. Other one-dimensional climate models show a similar sensitivity (Schneider 1972). Our model, however, has only CBL clouds rather than clouds at all levels as observed.

The equilibrium response of the CBL on these long timescales (Fig. 18) to mean wind change is considerably changed from Figs. 5 and 15. Cloud base still falls with wind speed, but the increase of θ_e is much reduced, and cloud top is almost flat near 800 mb. We

have plotted the corresponding SST (now coupled to ω_O) on the top axis, and its θ_{es} as long, light dashes; θ_e and cloud top now decrease with increasing equilibrium SST, the reverse of Figs. 3 and 13.

The increase in the latent heat flux with wind speed (Fig. 19) is now reduced still further from the tropospheric coupled case (shown dashed), while the surface Bowen ratio still decreases with increasing ω_O. Figures 16 and 19, which together show four different model curves for the dependence of the surface evaporation on wind speed, illustrate the perils of oversimple assumptions for the air–sea interaction process. Table 4 summarizes the gradient of LH with wind speed near 6.7 m s^{-1} for the four cases.

For the SST coupled case, the surface LH flux now *decreases* with increasing SST (top scale on Fig. 19), because the SST increase is an equilibrium response to decreased surface wind speed. This response of the fully coupled system has been seen in models (Druyan 1988), but is not well understood (Nicholson and Entekhabi 1988).

c. *Coupling of surface evaporation to SST changes*

Druyan (1988) noted a correlation between increased SST and reduced evaporation in a coupled ocean–climate model, but Nicholson and Entekhabi (1988) questioned whether this was physically reasonable. It is easy to see how confusion can arise because of the different coupling on different timescales. Figure 20 summarizes from Figs. 4, 14, and 19 (replotted) the change of LH flux with SST on three timescales. On the shortest timescale (dotted curve) of CBL radiative equilibrium (~1 day) with a fixed upper troposphere, the LH flux increases quite steeply with SST. With tropospheric energy balance (~10 days), the increase is halved to 6 W m^{-2} K^{-1} (dashed curve), while on the longest timescale, where the SST increase (rather than being externally specified) is a response to a decrease in wind speed, the surface evaporation actually decreases with SST at −10 W m^{-2} K^{-1}, as indicated by Druyan (1988).

TABLE 4. Slope of surface LH flux with wind-speed near 6.7 m s^{-1}.

Model	Units: W m^{-3} s^{-1}
Constant surface RH = 73.8%	22.5
Uncoupled CBL	7.1
Troposphere coupled CBL	3.9
SST and troposphere coupled CBL	1.7

d. *Climate model speculations*

Our model in its present form has clear limitations as a climate model. We have a fixed stratosphere (this could be relaxed), fixed cloudiness in the CBL (the coupling of cloudiness to CBL parameters is unclear), no upper-level clouds, and no atmospheric transports to midlatitudes. Some of these assumptions partly compensate. The atmospheric export to mid-latitudes (~20–30 W m^{-2}) implies that Eq. (14) is not satisfied exactly; but heating by upper-level clouds in the tropics (which we have also neglected) probably produces a roughly compensating error (Ramanathan 1987), as discussed in section 2h(3). An export of energy by the oceans from the tropics, equivalent to a net energy imbalance at the ocean surface of ≈18 W m^{-2}, was imposed in our model, together with a CBL cloud fraction of 25%. Nonetheless, it is of interest to see the response of the model to changes in solar flux and CO_2

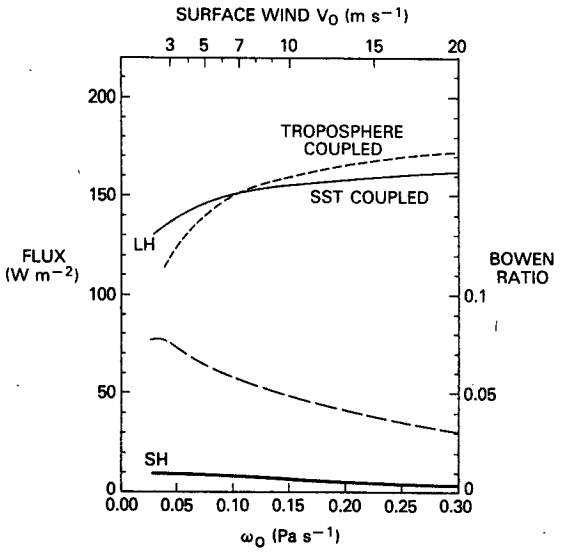

FIG. 19. As in Fig. 6 for coupled SST and troposphere. Short dashes show latent heat flux for coupled troposphere but fixed SST from Fig. 16.

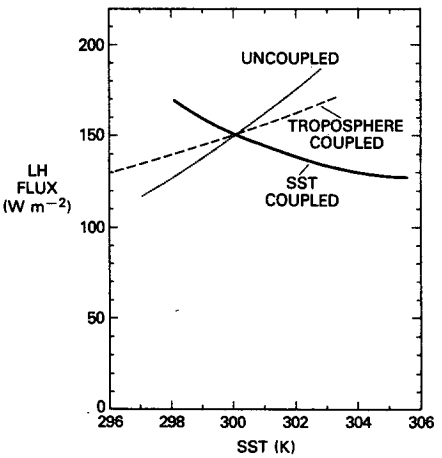

FIG. 20. Latent heat flux as a function of SST for the three solutions: uncoupled CBL (dotted), fully coupled troposphere (dashed) and coupled SST and troposphere (solid).

concentration, because the model can be regarded as a radiative–convective equilibrium model (RCM) (with an interactive CBL) for just the tropics, rather than the whole globe.

e. Response of SST to upper tropospheric moisture

An increase in upper tropospheric moisture reduces the radiative cooling of the troposphere. Table 5 shows the tropopause net radiative flux, and tropospheric net flux difference as a function of tropopause $\mathcal{P}_{TR}$ and relative humidity (with respect to water saturation) for a fixed SST = 300 K.

These flux changes have only a small effect on the tropospherically coupled solutions (section 4b), but a much larger effect with a coupled ocean. Figure 21 shows the equilibrium SST as a function of relative humidity at the tropopause, for a fixed ocean transport of 18 W m^{-2}, fixed CBL cloudiness and surface wind (ω_O = 0.1 Pa s^{-1}). The equilibrium SST increases sharply with the upper level humidity.

The tropical upper tropospheric relative humidity is not well known, and thin cirrus clouds are believed to be quite prevalent (which would indicate patches of high humidity). It is clear that our tuning of our base equilibrium SST to 300 K using CBL cloud function and oceanic export depends also on our choice of $\mathcal{P}_{TR}$ = −30 mb. For different values of $\mathcal{P}_{TR}$, the choice of the ocean export $X_O = N_{TR}$ in Table 4 gives a convenient way of tuning the SST to a 300 K reference value. This was done to study the response of the model to doubling CO_2 and changing solar constant.

f. SST response to CO_2 doubling and solar constant changes

We explored the SST response as a function of tropopause humidity, for a fixed surface wind of ω_O = 0.1 Pa s^{-1}. For each value of $\mathcal{P}_{TR}$, the oceanic export X_O was set equal to the net tropospheric flux, N_{TR} in Table 5, so as to give an equilibrium SST of 300 K with CO_2 = 330 ppm and a standard solar flux of 1360.3 W m^{-2}. The change of the tropical SST from this 300 K reference for a doubling of CO_2 (from 330 to 660 ppm) and a ±2% change in the solar constant is shown in Fig. 22, as a function of tropopause relative humidity. Figure 22 shows that the surface warming in the tropics for a 102% solar flux slightly exceeds that for a CO_2 doubling, and the warming increases with increasing tropopause humidity from about 2 to 3° K. With a reduction in solar constant, there is a cooling of similar magnitude, but the cooling does not increase as much at high tropopause humidities.

This range of values for the surface warming for a CO_2 doubling of 1.9 to 3.2° K (increasing with tropopause humidity) is comparable with that shown in general circulation climate models (GCMs) in the tropics (Schlesinger and Mitchell 1987, Rind 1987).

TABLE 5. Net tropopause flux (N_{TR}) and net tropospheric flux divergence (ΔN_{TR}) as a function of tropopause humidity.

$\mathcal{P}_{TR}$ (mb)	RH (%)	N_{TR} (W m^{-2})	ΔN_{TR} (W m^{-2})
−40	5	16.2	159.8
−30	11	18.2	158.1
−20	26	20.2	156.2
−10	53	22.4	154.6
0	100	24.5	152.7

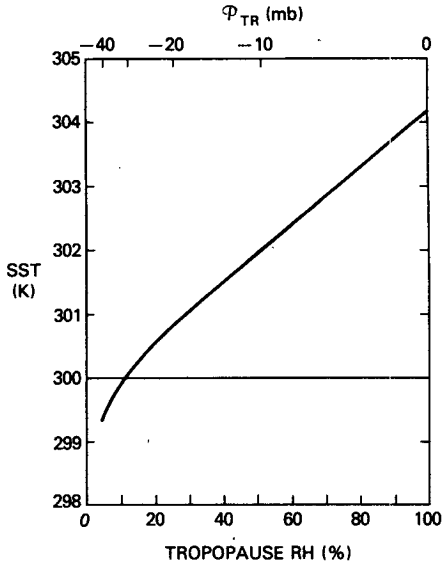

FIG. 21. SST as a function of tropopause relative humidity for coupled SST and troposphere.

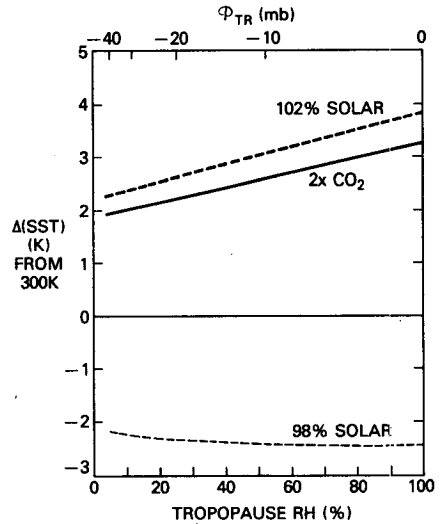

FIG. 22. Change of SST (from 300 K reference) for CO_2 doubling and ±2% change in solar constant, as a function of tropopause relative humidity.

Most GCMs show larger high-latitude surface warming, so that the global average is larger than the tropical value. The sensitivity of our result for the tropics to upper tropospheric humidity suggests that GCMs may have a similar sensitivity in the tropics to humidity or to the upper-level cloud parameterization. However, the assumptions about the oceanic export from the tropics and the other simplifications, discussed in section 5d, make our model results speculative for these climate problems.

6. Conclusions

We have developed a coupled radiative–convective boundary layer model, and used energy balance constraints to study CBL equilibrium, and surface fluxes on three timescales. In section 3 (Figs. 3–11), we showed the "uncoupled" CBL solutions: those with a specified SST, tropospheric thermodynamic structure and cloud-top subsidence parameter. These satisfy radiative equilibrium only for the CBL. They show an increase of CBL depth with increasing SST and a tight coupling of the low-level θ_e to the SST. The threshold for deep convection associated with SST > 27.5°C, observed in much of the Pacific and Indian Oceans (Graham and Barnett 1987), is probably related to low-level θ_e exceeding the deep tropospheric θ_{es} above the SST. With increasing surface wind, cloud base falls, while θ_e and cloud top both increase. The latent heat flux increases almost linearly at 11.1 W m^{-2} K^{-1} with SST, while the response to increasing wind is quite nonlinear, as the CBL structure adjusts. The slope near 6.7 m s^{-1} is only one-third of the linear slope assuming constant relative humidity (Table 4 and Fig. 6). Increasing the subsidence parameter suppresses the CBL, reduces θ_e and increases the surface latent heat flux for constant surface wind and SST. Cloud top is sensitive to the moisture above, which controls the radiative cooling of the CBL, and both cloud base and cloud top are sensitive to the surface Bowen ratio. The coupling of the sensible heat flux to the radiative cooling of the subcloud layer gives a tightly constrained sensible heat ~8–10 W m^{-2}, and a Bowen ratio ~ 0.06 for constant surface wind speed, similar to observed values for the undisturbed tradewinds. However, with increasing wind speed, cloud base falls, and with it the Bowen ratio falls also.

In section 4 we coupled the subsidence ($\omega_{T'}$) at CBL top to the deep tropospheric net radiative cooling, and the tropospheric temperature (θ_{es}) and moisture structure (q_T) to the low level θ_e. The model solutions of cloud base near 950 mb, cloud top and CBL top near 800 mb and a low level θ_e of 347 K are close to the tropical mean for an SST of 300 K. This gives us confidence in both the basic model structure and the radiation code. There are two major impacts of "tropospheric coupling" on the CBL structure and fluxes. The deepening of CBL with SST and surface wind was reduced significantly; first by the coupling of $\omega_{T'}$ and θ_{es}, and still further by the coupling of q_T. The surface latent heat flux increase with SST was halved to 5.6 W m^{-2} K^{-1}, giving a total surface heat flux increase close to the slope of the Planck function with SST. The slope of the latent heat flux with surface wind was almost halved to 4 W m^{-3} s by introducing tropospheric coupling (Table 4). In this case the surface fluxes can only increase as the CBL moistens and the longwave cooling of the troposphere increases. The results for the low level θ_e were fitted with a simple expression for the low-level air wet-bulb temperature.

$$T_{wO} = T_O - 24[1 + 0.008(300 - T_O)]/V_O. \quad (22)$$

The wet-bulb depression varies inversely with surface wind speed (V_O in m s^{-1}) and rather slowly with SST (T_O in K). A similar approximate formula was given for cloud base (in mb).

$$p_B = p_O - 390[1 + 0.035(300 - T_O)]/V_O. \quad (23)$$

These formulae could be checked empirically using climatic data. We discussed the coupled interactions between boundary layer thermodynamic structure, radiative cooling, stability and CBL depth, which lead to the requirement for a fully coupled model to predict boundary layer depth. Our solutions are perhaps the first for the CBL structure and fluxes, which include a full radiative coupling.

In section 5 we specified the radiative flux at the tropopause, equivalent to imposing an oceanic energy export from the tropics, and found the equilibrium SST and CBL structure on long time scales. The equilibrium SST falls nonlinearly with increasing surface wind (Fig. 17), as the surface evaporation is forced. However, the slope of the surface latent heat flux with wind speed is now reduced still further to only 1.7 W m^{-3} s (near 6.7 m s^{-1}) as the SST and CBL structure adjust. The equilibrium CBL top is now very flat with wind speed near 800 mb, and θ_e only increases weakly with wind speed, from 347 to 350 K. Cloud base, however, still falls with wind speed. Because SST now falls with increasing wind speed, the latent heat flux *falls* with increasing SST for the ocean-coupled solution: in sharp contrast to the increased surface evaporation with SST for the tropospheric-coupled solution (Fig. 20). We then turned to some simple climate model solutions. The tropopause humidity remains an important specified parameter: we show that the equilibrium SST increases quite sharply with upper tropospheric humidity. We then show the increase in the tropical SST from a reference of 300 K for a CO_2 doubling and a ±2% change in solar constant as a function of tropopause humidity. For a CO_2 doubling, the tropical SST warms 1.9 to 3.2° K as the tropopause humidity increases towards (water) saturation. This is comparable to tropical values given by GCMs. The increase in SST is slightly higher for a 2% increase in solar constant. This tropical model may be of value as a radiative–

convective model for comparison with GCM simulations of climate. In its present form, it has serious limitations as a climate model (namely, a specified stratosphere, specified CBL cloud fraction, no upper level clouds and tropospheric energy export from the tropics, and a specific oceanic export). On the other hand, in comparison with other radiative–convective models, it has a partly cloudy boundary layer with interactive cloud liquid water and optical properties; and the solutions depend on a mean surface speed and have an implied tropospheric circulation.

Acknowledgments. This research was supported by the National Science Foundation under Grant ATM87-05403 and by the NASA Goddard Space Flight Center under Contract NAS5-30524. I am grateful to J. Coakley for helpful discussions, and to reviewers for comments.

APPENDIX A

Subcloud Layer Closure

The validity of the closure (11) has been quite well established for dry convective boundary layers (without cloud) in terms of buoyancy flux: the virtual potential temperature flux.

$$F_{B\theta V} = -k_v F_{O\theta v} \quad \text{with} \quad k_v \approx 0.2 \qquad (11')$$

Many authors have used this closure (11′) in studies of the subcloud layer (Betts 1976; LeMone and Pennell 1976; Nicholls and LeMone 1980). The difference between (11) and (11′) is important over the oceans because the contribution of the latent heat fluxes to the buoyancy flux is comparable to that of the surface sensible heat flux. However we shall use (11) not (11′) for three reasons. First, it is simpler and directly couples surface sensible heat flux to the radiative cooling of the subcloud layer. The second reason is our lack of understanding of fractional cloudiness and the implicit coupling of the convective and radiative fluxes within the CBL (Betts and Ridgway 1988); ΔN_B for the subcloud layer is almost directly proportional to cloud fraction, so that cloud fraction is a crucial unknown, which we are here specifying. The third related reason is uncertainty as to whether (11′) is really valid for partially cloudy layers. There has been extensive discussion as to whether it can be adapted in any form for stratocumulus (Kahn and Businger 1979; Lilly and Schubert 1980; Deardorff and Businger 1980), and by inference it is questionable for cumulus layers. Most of the observational support comes from aircraft studies selected to have very little cloudiness.

REFERENCES

Albrecht, B. A., 1979: A model of the thermodynamic structure of the trade wind boundary layer Part II: Applications. *J. Atmos. Sci.*, **36**, 90–98.

——, 1984: A model study of downstream variations of the thermodynamic structure of the trade winds. *Tellus*, **36A**, 187–202.

——, A. K. Betts, W. Schubert and S. K. Cox, 1979: A model of the thermodynamic structure of the trade-wind boundary layer: Part I Theoretical formulation and sensitivity tests. *J. Atmos. Sci.*, **35**, 73–89.

——, V. Ramanathan and B. A. Boville, 1986: The effects of cumulus moisture transports on the simulation of climate with a general circulation model. *J. Atmos. Sci.*, **43**, 2443–2462.

Augstein, E., 1978: The atmospheric boundary layer over the tropical oceans. *Meteorology over the Tropical Oceans*. D. B. Shaw, Ed., Roy. Meteor. Soc., 73–104.

——, H. Riehl, F. Ostapoff and V. Wagner, 1973: Mass and energy transports in an undisturbed Atlantic trade wind flow. *Mon. Wea. Rev.*, **101**, 101–111.

——, H. Schmidt and F. Ostapoff, 1974: The vertical structure of the atmospheric planetary boundary layer in undisturbed trade winds over the Atlantic Ocean. *Bound. Layer Met.*, **6**, 129–150.

——, and M. Wendel, 1980: Modelling of the time dependent atmospheric boundary layer with non-precipitating cumulus clouds. *Beitr. Phys. Atmos.*, **53**, 509–538.

Betts, A. K., 1973: Non-precipitating convection and its parameterization. *Quart. J. Roy. Meteor. Soc.*, **99**, 178–196.

——, 1975: Parameteric interpretation of trade wind cumulus budget studies. *J. Atmos. Sci.*, **32**, 1934–1945.

——, 1976: Modelling subcloud layer structure and interaction with a shallow cumulus layer. *J. Atmos. Sci.*, **33**, 2363–2382.

——, 1982a: Saturation point analysis of moist convective overturning. *J. Atmos. Sci.*, **39**, 1484–1505.

——, 1982b: Cloud thermodynamic models in salt water point coordinates. *J. Atmos. Sci.*, **39**, 2182–2191.

——, 1983: Thermodynamics of mixed stratocumulus layers; saturation point budgets. *J. Atmos. Sci.*, **40**, 2655–2670.

——, 1985: Mixing line analysis of clouds and cloudy boundary layers. *J. Atmos. Sci.*, **42**, 2751–2763.

——, 1986: A new convective adjustment scheme. Part I: Observational and theoretical basis. *Quart. J. Roy. Meteor. Soc.*, **112**, 677–692.

——, and B. A. Albrecht, 1987: Conserved variable analysis of boundary layer thermodynamic structure over the tropical oceans. *J. Atmos. Sci.*, **44**, 83–99.

——, and J. Simpson, 1987: Thermodynamic budget diagrams for the hurricane subcloud layer. *J. Atmos. Sci.*, **44**, 842–849.

——, and W. Ridgway, 1988: Coupling of the radiative, convective and surface fluxes over the equatorial Pacific. *J. Atmos. Sci.*, **45**, 522–536.

Byers, H. R., and R. K. Hall, 1955: A census of cumulus cloud height versus precipitation in the vicinity of Puerto Rico during the winter and spring of 1953–54. *J. Meteor.*, **12**, 176–178.

Cess, R. D., 1976: Climate change: an appraisal of atmospheric feedback mechanisms employing zonal climatology. *J. Atmos. Sci.*, **33**, 1831–1843.

Deardorff, J. W., 1980: Cloud-top entrainment instability. *J. Atmos. Sci.*, **37**, 131–147.

——, and J. A. Businger, 1980: Comments on "Marine Stratocumulus convection. Part I: Governing equations and horizontally homogenous solutions." *J. Atmos. Sci.*, **37**, 481–482.

Druyan, L., 1988: Comments on "Rainfall variability in equatorial and Southern Africa: relationships with sea surface temperatures along the Southwestern coast of Africa." *J. Climate*, **1**, 569.

Emanuel, K. A., 1988a: The maximum intensity of hurricanes. *J. Atmos. Sci.*, **45**, 1143–1155.

——, 1988b: Towards a general theory of hurricanes. *Amer. Sci.*, **76**, 371–379.

Firestone, J. K., and B. A. Albrecht, 1986: The structure of the atmospheric boundary layer in the central equatorial Pacific during January and February of FGGE. *Mon. Wea. Rev.*, **114**, 2219–2231.

Fouquart, Y., 1985: Radiation in boundary layer clouds. Report of the JSC/CAS Workshop on Modelling of Cloud Topped Boundary Layer, Fort Collins, Colorado, 22–26 April 1985, Appendix D. [Available from Dept. of Atmos. Sci., Colorado State University, Fort Collins, CO 80523].

Fravalo, C., Y. Fouquart and R. Rosset, 1981: The sensitivity of a model of low stratiform clouds to radiation. *J. Atmos. Sci.*, **38**, 1049–1062.

Gadgil, S., P. V. Joseph and N. V. Joshi, 1984: Ocean–atmosphere coupling over monsoon regions. *Nature*, **312**, 141–143.

Graham, N. E., and T. P. Barnett, 1987: Sea surface temperature, surface wind divergence and convection over the tropical oceans. *Science*, **238**, 657–659.

Hanson, P. H., 1981: On mixing by trade-wind cumuli. *J. Atmos. Sci.*, **38**, 1003–1014.

——, 1987: Response of marine atmospheric boundary layer height to sea surface changes: Mixed layer theory. *J. Geophys. Res.*, **92**, 8226–8230.

Harshvardhan, R. Davies, D. A. Randall and T. G. Corsetti, 1987: A fast radiation parameterization for atmospheric circulation models. *J. Geophys. Res.*, **92**, 1009–1016.

Heckley, W. A., 1985: Systematic errors in the ECMWF operational forecasting model in tropical regions. *Quart. J. Roy. Meteor. Soc.*, **111**, 709–738.

Holland, J. Z., and E. Rasmusson, 1973: Measurements of the atmospheric mass energy and momentum budgets over a 500 kilometer square of tropical ocean. *Mon. Wea. Rev.*, **101**, 44–55.

Kahn, P. H., and J. A. Businger, 1979: The effect of radiative flux divergence on entrainment of a saturated convective boundary layer. *Quart. J. Roy. Meteor. Soc.*, **105**, 303–306.

Lal, M., and V. Ramanathan, 1984: The effects of moist convection and water vapour radiative processes on climate sensitivity. *J. Atmos. Sci.*, **41**, 2238–2249.

LeMone, M. A., and W. T. Pennell, 1976: The relationship of trade-wind cumulus distribution to subcloud layer fluxes and structure. *Mon. Wea. Rev.*, **104**, 524–539.

Lilly, D. K., and W. H. Schubert, 1980: The effects of radiative cooling in a cloud-topped mixed layer. *J. Atmos. Sci.*, **37**, 482–487.

Ludlam, F. H., 1980: *Clouds and Storms.* Pennsylvania State University Press, 405 pp.

Malkus, J. S., 1956: On the maintenance of the tradewinds. *Tellus*, **8**, 335–350.

—— 1962: Large-scale interactions. Chapter 4. *The Sea*, Vol. 1: *Ideas and Observations on Progress in Study of the Sea.* M. N. Hill, Ed., *Wiley-Interscience*, 88–294.

Neiburger M., 1960: The relationship of air mass structure to the field of motion over the eastern North Pacific in summer. *Tellus*, **12**, 31–40.

Nicholls, S., and M. A. LeMone, 1980: The fair weather boundary layer in GATE: The relationship of subcloud fluxes and structure to the distribution and enhancement of cumulus clouds. *J. Atmos. Sci.*, **37**, 2051–2067.

Nicholson, S. E., and E. E. Entekhabi, 1988: Reply (to Druyan 1988). *J. Climate*, **1**, 570.

Nitta, T., and S. Esbensen, 1974: Heat and moisture budgets using BOMEX data. *Mon. Wea. Rev.*, **102**, 17–28.

Ogura Y., J. Russell and H-R Cho, 1977: A semi-emipirical model of the tradewind inversion. *J. Met. Soc. Japan*, **55**, 209–222.

Palmen, E., 1948: On the formation and structure of tropical cyclones. *Geophysica*, **3**, 26–28.

Paulson, C. A., E. Levitt and R. G. Fleagle, 1972: Air–sea transfer of momentum, heat and water determined from profile measurements during BOMEX. *J. Phys. Oceanogr.* **2**, 487–497.

Pond, S., G. T. Phelps, J. E. Paquin, G. McBean and R. W. Stewart, 1971: Measurements of the turbulent fluxes of momentum moisture and sensible heat over the ocean. *J. Atmos. Sci.*, **28**, 901–917.

Ramanathan, V, 1981: The role of ocean–atmosphere interactions in the CO_2 climate problem. *J. Atmos. Sci.*, **38**, 918–930.

———, 1987: The role of earth radiation budget studies in climate and general circulation research. *J. Geophys. Res.*, **92**, 4075–4095.

——, 1988: The greenhouse theory of climate change: A test by an inadvertent global experiment. *Science*, **240**, 293–299.

Randall, D. A., 1980: Conditional instability of the first kind upside-down. *J. Atmos. Sci.*, **37**, 125–130.

Riehl, H., T. C. Yeh, J. S. Malkus and N. E. LaSeur, 1951: the Northeast trade of the Pacific Ocean. *Quart. J. Roy. Meteor. Soc.*, **77**, 598–626.

——, and J. S. Malkus, 1958: On the heat balance of the equatorial trough zone. *Geophys.* **6**(3), 503–538.

——, and J. Simpson, 1979: The heat balance of the equatorial trough zone: revisited. *Contrib. Atmos. Phys.*, **52**, 287–305.

Rind, D., 1987: The doubled CO_2 Climate: Impact of the sea surface temperature gradient. *J. Atmos. Sci.*, **44**, 3235–3268.

Sarachik, E. S., 1978: Tropical sea surface temperature: an interactive one-dimensional atmosphere ocean model. *Dyn. Atmos. Oceans*, **2**, 455–469.

Schubert, W. H., 1976: Experiments with Lilly's cloud-topped mixed layer model. *J. Atmos. Sci.*, **33**, 436–446.

Schlesinger, M. E., and J. F. B. Mitchel, 1987: Climate model simulations of the equilibrium climatic response to increased carbon dioxide. *Rev. Geophys.*, **25**, 760–798.

Schubert, W. H., J. S. Wakefield, E. J. Steiner and S. K. Cox, 1979: Marine stratocumulus convection. Part I: Governing equations and horizontally homogeneous solutions. *J. Atmos. Sci.*, **36**, 1286–1307.

Schneider, S. H., 1972: Cloudiness as a global climatic feedback mechanism; the effects of the radiation balance and surface temperature of variations of cloudiness. *J. Atmos. Sci.*, **29**, 1413–1422.

Stage, S. A., and J. A. Businger, 1981: A model for entrainment into a cloud-topped boundary layer. Part I: Model description and application to a cold air outbreak. *J. Atmos. Sci.*, **38**, 2213–2229.

Stephens, G. L., 1978: Radiation Profiles in extended water clouds. II: Parameterization schemes. *J. Atmos. Sci.*, **35**, 2123–2132.

——, G. G. Campbell and T. H. VonderHaar, 1981: Earth radiation budget measurements from satellites and their interpretation for climate modelling and studies. *J. Geophys. Res.*, **86**, 9739–9760.

VonderHaar, T. H., and A. H. Oort, 1973: New estimates for the poleward energy transport by Northern Hemispheric oceans. *J. Phys. Oceanogr.*, **3**, 169–172.